Stem Cell Reports
Article
ISSCR
OPEN ACCESS

Absence of Both Thyroid Hormone Transporters MCT8 and OATP1C1 Impairs Neural Stem Cell Fate in the Adult Mouse Subventricular Zone

Cristina Luongo,[1,4] Lucile Butruille,[1,4] Anthony Sébillot,[1] Karine Le Blay,[1] Markus Schwaninger,[2] Heike Heuer,[3] Barbara A. Demeneix,[1] and Sylvie Remaud[1,*]
[1]UMR 7221 Phyma, CNRS/Muséum National d'Histoire Naturelle, 75005 Paris, France
[2]Institute for Experimental and Clinical Pharmacology and Toxicology, University of Lübeck, 23562 Lübeck, Germany
[3]Department of Endocrinology, Diabetes and Metabolism, University of Duisburg-Essen, 45122 Essen, Germany
[4]These authors contributed equally
*Correspondence: sremaud@mnhn.fr
https://doi.org/10.1016/j.stemcr.2020.12.009

SUMMARY

Adult neural stem cell (NSC) generation in vertebrate brains requires thyroid hormones (THs). How THs enter the NSC population is unknown, although TH availability determines proliferation and neuronal versus glial progenitor determination in murine subventricular zone (SVZ) NSCs. Mice display neurological signs of the severely disabling human disease, Allan-Herndon-Dudley syndrome, if they lack both MCT8 and OATP1C1 transporters, or MCT8 and deiodinase type 2. We analyzed the distribution of MCT8 and OATP1C1 in adult mouse SVZ. Both are strongly expressed in NSCs and at a lower level in neuronal cell precursors but not in oligodendrocyte progenitors. Next, we analyzed *Mct8*/*Oatp1c1* double-knockout mice, where brain uptake of THs is strongly reduced. NSC proliferation and determination to neuronal fates were severely affected, but not SVZ-oligodendroglial progenitor generation. This work highlights how tight control of TH availability determines NSC function and glial-neuron cell-fate choice in adult brains.

INTRODUCTION

In the adult mammalian brain, a pool of neural stem cells (NSCs) persists in two well-defined neurogenic regions: the subgranular zone (SGZ) of the hippocampus and the subventricular zone (SVZ) lining the lateral ventricles. Adult neurogenesis and oligodendrogenesis are complex processes that involve proliferation and differentiation of both neuronal and oligodendrocyte progenitors derived from NSCs. In rodents, newly generated SVZ-neuroblasts migrate tangentially toward the olfactory bulbs (OBs) where they differentiate into interneurons that participate in olfaction (Breton-Provencher et al., 2009; Enwere et al., 2004). SVZ-derived oligodendrocyte precursor cells (OPCs) migrate radially into the overlying white matter (e.g., the corpus callosum).

Under physiological conditions, SVZ-NSCs generate principally neuronal precursor cells (Menn et al., 2006). However, SVZ-NSCs can also generate a few oligodendrocytes *in vitro* and *in vivo* (Menn et al., 2006). The balance between NSC-derived neurons and oligodendrocytes is modulated by several physiological and pathological stimuli. For example, after a demyelinating lesion (characterized by a loss of myelinating oligodendrocytes, a hallmark of several white matter diseases such as multiple sclerosis), the generation of new SVZ-derived OPCs is favored to stimulate myelin repair (Nait-Oumesmar et al., 2007; Remaud et al., 2017; Xing et al., 2014). Thus, understanding how NSC fate decision (neurons versus glia) is modulated in the adult brain could have significant implications for neurodegenerative diseases when new neurons and/or glia are needed to promote brain repair.

T_3, the biologically active form of THs, is essential for brain development in all vertebrates, including humans. In the murine brain, it has recently been established that T_3 also regulates adult neurogenesis and especially NSC fate decision between neurons and glia. In the SGZ, T_3 increases neuronal differentiation by enhancing proneural gene expression (Fanibunda et al., 2018; Kapoor et al., 2012, 2015). In the SVZ, T_3 drives NSC fate preferentially toward a neuronal fate, while a transient lack of T_3 favors the generation of new OPCs capable of functional remyelination (Remaud et al., 2017).

Local control of TH availability is crucial for spatiotemporal control of TH action, in particular within the NSC niches (Mayerl et al., 2020; Remaud et al., 2017). Numerous factors control TH availability in the brain from TH transporters (THTs) (Friesema et al., 2003, Friesema et al., 2008; Pizzagalli et al., 2002), to inactivation/activation by deiodinases (Bianco and Kim, 2006; Luongo et al., 2019), presence of receptors for TH (Flamant and Gauthier, 2013), and even co-activators/corepressors (Astapova and Hollenberg, 2013; Suzuki et al., 2007). SVZ-derived OPCs are protected from the neuralizing effects of T_3 through the expression of the T_3-inactivating enzyme deiodinase type 3 (*Dio3*) and the absence of the T_3-receptor TRα1. In contrast, TRα1 was strongly expressed in neuronal progenitors, whereas *Dio3* was not (Remaud et al., 2017). However, cell-membrane transporters (THTs) facilitating TH uptake represent an additional level controlling intracellular TH availability, potentially influencing NSC fate decision too, but their involvement is as yet unknown.

THTs facilitate TH uptake into different cell types, including glial and neuronal cells. The importance of THTs for brain function is illustrated by patients carrying inactivating mutations in the *Slc16a2* gene encoding the monocarboxylate transporter 8 (*Mct8*). These patients suffer from a severe form of psychomotor retardation (Allan-Herndon-Dudley syndrome [AHDS]) combined with abnormal serum TH levels (high T_3, low T_4) (Dumitrescu et al., 2004; Friesema et al., 2004; Groeneweg et al., 2019). Recently, it has been shown that, in humans, mutations in the organic anion transporting polypeptide 1C1 (OATP1C1) decrease T_4 uptake and are associated with developmental impairments that later evolve to neurodegenerative disease (Strømme et al., 2018). Mice deficient in MCT8 (*Mct8* knockout [KO]) faithfully recapitulate the peripheral altered TH serum levels observed in humans, but do not display neurobehavioral deficits, while they suffer from mild brain hypothyroidism (Trajkovic et al., 2007a). It is well established that OATP1C1 cooperates with MCT8 to facilitate TH transport across the blood-brain barrier (BBB) and/or the blood-cerebrospinal fluid barrier into the rodent brain. Mice deficient for both MCT8 and OATP1C1 (*Mct8/Oatp1c1* or double knockout [DKO]) exhibit central TH deficiency associated with locomotor abnormalities similar to those found in MCT8-deficient patients, showing that this DKO mouse is a suitable model especially for the neurological component of AHDS (Mayerl et al., 2014). To be more precise, only DKO mice display a strong decrease of both T_3 and T_4 contents in the brain as a consequence of a highly reduced T_4 and T_3 transport across brain barriers (Mayerl et al., 2014). This allowed us to compare the cellular effects underlying the absence of both transporters with our previous well-established data obtained after induction of adult-onset hypothyroidism (Gothié et al., 2017a; Remaud et al., 2017; Vancamp et al., 2019).

Here, we determined how the lack of MCT8 and/or OATP1C1 affects NSC fate in the adult mouse brain. We demonstrate that both THTs are strongly expressed in NSCs and in committed neuronal precursors but not in oligodendroglial lineage cells. Furthermore, using DKO mice, we show that THTs regulate neuronal lineage progression, and that their absence leads to impairments in olfactory function. In contrast, the generation of new OPCs derived from SVZ-NSCs is unaffected by the absence of THTs.

RESULTS

MCT8 and OATP1C1 Are Both Expressed in NSCs and Are Retained Mainly by Committed Neuronal Precursors within the Adult SVZ

Local TH availability is tightly regulated, permitting precise temporal and cell-specific control of TH action in the central nervous system. Cell-specific TH availability is determined by (1) a balance between TH-activating (mainly *Dio2* in the brain) and inactivating (*Dio3*) deiodinases enzymes, (2) cell-specific membrane THTs, (3) ligand (T_3)-dependent nuclear receptor (TR) forms (mainly *Thra1* within the adult SVZ; López-Juárez et al., 2012).

To elucidate the roles of MCT8 and OATP1C1 in adult SVZ neurogenesis, we first determined which SVZ cell types express these THTs by immunohistochemistry (IHC) (Figure 1). To detect OATP1C1 expressing cells *in vivo*, we used the OATP1C1:YFP reporter mouse (see Experimental Procedures), which exhibits a stronger signal (fluorescence in the cytosol) than the antibody directed against OATP1C1 (fluorescence of membrane-bound OATP1C1). Alternatively, we used this antibody to detect endogenous expression of OATP1C1 *in vitro* using neurosphere cultures. We observed that MCT8 (Figure 1A) and OATP1C1 (YFP+, Figure 1B) were highly expressed in NSCs co-expressing GFAP (pink) and SOX2 (red) in the adult SVZ, as was also confirmed in single cells dissociated from *in vitro* neurospheres (see the dotted signal in Figure S1A). MCT8 staining was absent in both the dorsal and lateral part of the SVZ in *Mct8* KO mice (Figure S1B), confirming the specificity of the MCT8 antibody. The specificity of the OATP1C1 antibody was previously demonstrated (Mayerl et al., 2012). Moreover, and as expected, MCT8 and OATP1C1 were mainly expressed on the plasma membrane as shown *in vitro* by the colocalization with the plasma membrane marker pan-cadherin and by the 3D reconstruction (Figure S1C).

Second, we observed that both MCT8 (Figure 1C) and OATP1C1 (Figure 1D) signals were detected at a low level in cells that expressed the neuronal markers DLX2 and DCX, respectively labeling early neuronal precursors and mature neuroblasts, whereas few (5%) oligodendroglial precursors (OLIG2+ SVZ-OPCs) expressed them. Altogether, these data indicate that MCT8 and OATP1C1 transporters are strongly expressed in NSCs, and are retained by neuronal lineage cells, while largely absent from precursors of the oligodendroglial lineage.

The TH Signaling Pathway Is Dynamically Regulated during Neurogenesis

To further characterize the mRNA expression patterns of THTs and other TH signaling pathway components in the different adult SVZ cell types, we performed RT-qPCR on fluorescence-activated cell sorting (FACS)-purified SVZ populations at each stage of the neuronal lineage (Figure 2A). To this end, we purified NSCs (quiescent NSCs CD133+EGFR− and activated NSCs CD133+EGFR+), transient amplifying cells or TACs (EGFR+), immature and migrating neuroblasts (EGFR+CD24+ and EGFR-CD24+, respectively). The purity of each FACS-purified SVZ cell

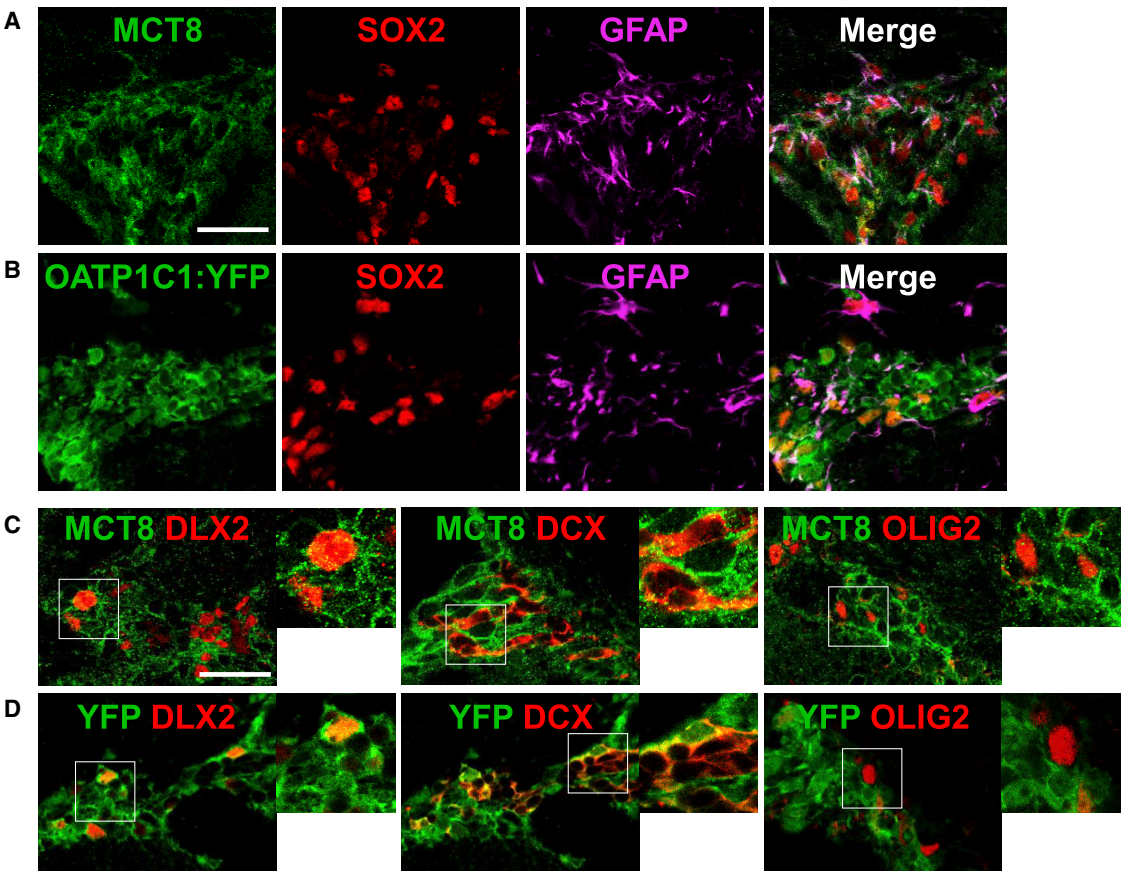

Figure 1. MCT8 and OATP1C1 Are Strongly Expressed in NSCs and Are Maintained Principally in Committed Neuronal Cells within the Adult SVZ

(A and B) Expression of MCT8 and OATP1C1 THTs in NSCs. MCT8 (A) and OATP1C1 (B) stainings on coronal section of adult dorsal SVZ show strong expression of both THTs in SOX2+ and GFAP+ NSCs.

(C and D) Expression of THTs in neuronal (DLX2+, DCX+) and oligodendrocyte (OLIG2+) differentiation pathways. MCT8 (C) and OATP1C1-YFP (D) are maintained in the neuronal differentiation pathway but are not expressed in the oligodendrocyte differentiation pathway. Scale bar: 30 μm.

population was confirmed by the expression of cell-type-specific marker genes by RT-qPCR (Figure S2). Statistical results are presented in Table S1. As expected, *Gfap* (Figure S2A) and *Nestin* (Figure S2B) expressions were limited to NSCs, whereas *Egfr* (Figure S2C) was mainly expressed in highly proliferative TAC progenitors. Early and late neuronal lineage cell markers (*Dlx2*, Figure S2D, and *Dcx*, Figure S2E, respectively) were detected in young and mature neuroblasts. Then, we assessed the gene expression profiles of several components of the TH signaling pathway in each isolated cell population. *Mct8* (*Slc16a2*, Figure 2B) and *Oatp1c1* (*Slco1c1*, Figure 2C) mRNA expressions were strongly expressed in NSCs and almost undetectable in TACs and committed neuronal precursors. This discrepancy between mRNA and protein expressions can be explained by a longer half-life of both THT proteins, as previously observed in rats (Wittmann et al., 2015). Similarly, we previously demonstrated that *Ttr* transcripts are expressed in the SVZ of adult mice, whereas the protein is not detected by IHC (Vancamp et al., 2019).

Two other key THTs, *Mct10* (*Slc16a10*, Figure 2D) and *Lat2* (*Slc7a8*, Figure 2F), had the opposite profile, with a higher expression in young and mature neuroblasts compared with low expression in both NSCs and TACs. The moderate expression of *Lat1* (*Slc7a5*, Figure 2E) was unchanged in the different SVZ cell types. Both *Thra* α1 (Figure 2G) and α2 (Figure 2H) isoforms were highly expressed in NSCs, significantly decreased in proliferating TACs, and then increased again in neuroblasts.

To assess in which cell type the TH signaling is preferentially activated, we quantified the expression of *Klf9* (Figure 2I), a well-known TH target gene (Hu et al., 2016). We

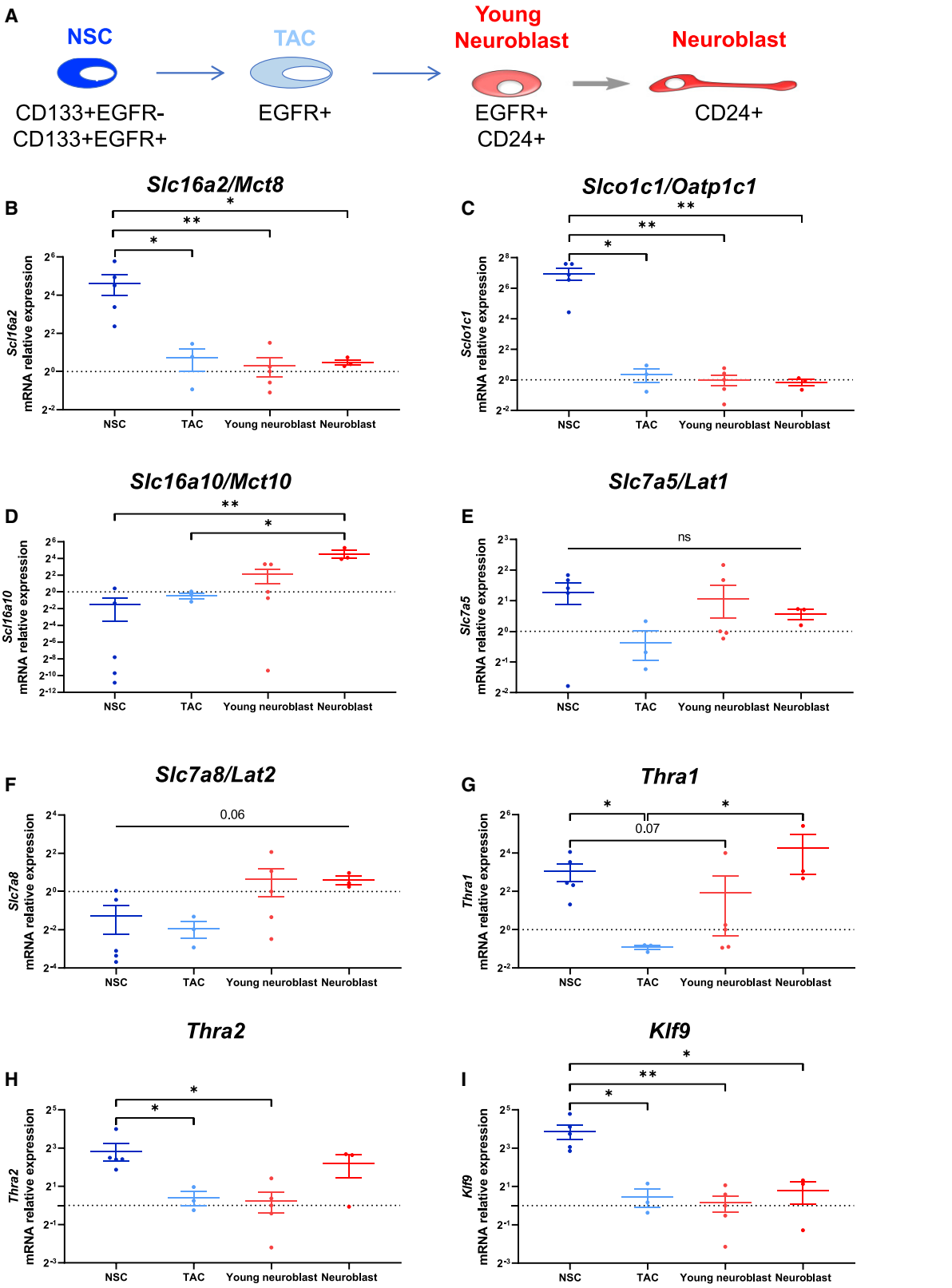

(legend on next page)

found that *Klf9* was highly expressed in NSCs and decreased in more committed cell types.

Taken together, the data show a dynamic expression pattern of several TH components during neuronal lineage specification, indicating a high TH responsiveness, especially in NSCs.

The Absence of MCT8 and OATP1C1 Impairs NSC Density and Self-Renewal Potential

As the above results suggest that both THTs are strongly expressed in adult NSCs, we next examined the functional properties of DKO-derived NSCs (Figure 3). A first observation was that the density of SOX2+ cells (Figure 3A), a pluripotency marker of both NSCs and progenitors, was reduced in the lateral SVZ of DKO mice compared with wild-type (WT) littermates (WT, 1,156 ± 95.07; DKO, 39.26 ± 4.99; t test, $p < 0.0001$, $t = 11.73$, $df = 16$; Figure 3B). Then, we tested if the proliferative potential of SOX2+ cells was affected in DKO mice. To this end, we performed IHC for SOX2 and KI67 (a cell proliferative associated marker, Figure 3A) to identify cycling progenitors. The density of SOX2+KI67+ cells was reduced in the SVZ of DKO mice compared with WT littermates (WT, 350.9 ± 29.5; DKO, 175.6 ± 24.32; t test, $p = 0.0003$, $t = 4.59$, $df = 16$; Figure 3C), suggesting that the proliferative neural stem/progenitor cell pool of the SVZ is impaired in the absence of both THTs. Accordingly, one day after plating neurosphere-dissociated cells (Figure 3D), we observed a 2-fold reduction of SOX2+KI67+ GFAP+ NSCs, showing that there were fewer cycling SVZ-NSCs in DKO mice (WT, 62.45 ± 4.68; DKO, 32.68 ± 5.59; Mann-Whitney test, $p = 0.0002$, $U = 203.5$; Figure 3E). The alteration observed in the SOX2+ population could be a consequence of a decreased self-renewal potential.

To test this hypothesis, we performed a neurosphere clonal assay. We determined self-renewal capacity by counting the number of neurospheres plated at a clonal density of 10,000 cells/mL over serial clonal passaging (from passages II to IX; Figure 3F). The number of neurospheres from WT and DKO SVZ were similar at passage II (DKO-neurosphere II [NS II], 0.93 ± 0.04; Bonferroni's test following two-way ANOVA, $p > 0.99$, $t = 1.02$; Figure 3G). However, after nine passages, WT versus DKO neurospheres revealed distinct NSC behaviors (Bonferroni's test, $p = 0.0003$, $t = 7.75$). As expected (Yoshioka et al., 2015), neurosphere numbers derived from WT mice drop strongly beyond the ninth passage (WT-neurosphere IX [NS IX], 0.24 ± 0.08; Bonferroni's test, $p < 0.0001$, $t = 10.37$). In contrast, DKO mice generated a large number of neurospheres forming NSCs that could be passaged extensively (DKO-NS II, 0.93 ± 0.04; DKO-NS IX, 0.81 ± 0.05; Bonferroni's test, $p = 0.89$, $t = 1.6$; Figure 3G). Therefore, neurospheres derived from DKO mice had an enhanced self-renewal capacity, continuing to propagate beyond the ninth passage. These results show that MCT8 and/or OATP1C1 exert key roles in self-renewal and maintenance of SVZ-NSCs in adult mice.

Loss of MCT8 and OATP1C1 Impairs Regulation of NSC Lineage Determination and Olfactory Behavior

Then, we determined consequences of the combined absence of both THTs on the generation of new neuronal versus oligodendroglial precursors derived from SVZ-NSCs *in vivo*. First, we quantified the density of uncommitted (DLX2+, DCX−) and committed (DLX2+, DCX+) NPCs, neural progenitor cells and mature neuroblasts (DLX2−, DCX+) in the SVZ of WT and DKO mice by IHC on coronal sections (Figure 4A). In DKO mice, the density of uncommitted and committed NPCs was significantly decreased as compared with WT mice (DLX2: WT, 130.7 ± 15.55 cells/mm^2; DKO, 53.03 ± 8.24 cells/mm^2; t test, $p = 0.002$, $t = 3.46$, $df = 30$; Figure 4B. DLX2-DCX: WT, 213.4 ± 20.04 cells/mm^2; DKO, 132.6 ± 20.39 cells/mm^2; t test, $p = 0.02$, $t = 2.57$, $df = 30$; Figure 4C). Surprisingly, the density of DCX+ mature neuroblasts is higher in DKO mice in comparison with controls (WT, 256.8 ± 32.14 cells/mm^2; DKO, 401 ± 55.81 cells/mm^2; t test, $p = 0.02$, $t = 2.41$, $df = 30$; Figure 4D).

The accumulation of neuroblasts in the SVZ of DKO mice may reflect hampered or delayed migration of mature neuroblasts, and so we investigated whether the loss of MCT8 and OATP1C1 affected SVZ-NPC migration. To this end, neurospheres generated from SVZ of WT and DKO mice were plated on eight-well glass slides (Millicell) coated with poly-D-lysine (Sigma). Their migration behavior was

Figure 2. TH Signaling Components Are Dynamically Expressed in Neuronal Lineage Cells within the Adult SVZ

(A) Schematic representation of the markers used to quantify TH signaling components mRNA expression levels in quiescent and activated NSCs (CD133+EGFR), TACs (EGFR+), NPCs (EGFR+CD24+) and neuroblasts (CD24+) from FACS-sorted SVZ cells of five adult WT male mice.

(B–F) Detection of THTs mRNA expression levels in FACS-sorted SVZ cells: *Slc16a2/Mct8* (B), *Slco1c1/Oatp1c1* (C), *Slc16a10/Mct10* (D), *Slc7a5/Lat1* (E), *Slc7a8/Lat2* (F).

(G and H) Detection of TH receptor mRNA expression levels in FACS-sorted SVZ cells: *Thra1* (G) and *Thra2* (H).

(I) Gene expression analysis of TH-responsive gene *Klf9*. n = 3–5 samples per cell population, Kruskal-Wallis test followed by permutation test, *$p < 0.05$, **$p < 0.01$. Data are presented in boxplots with medians, minimum, and maximum values.

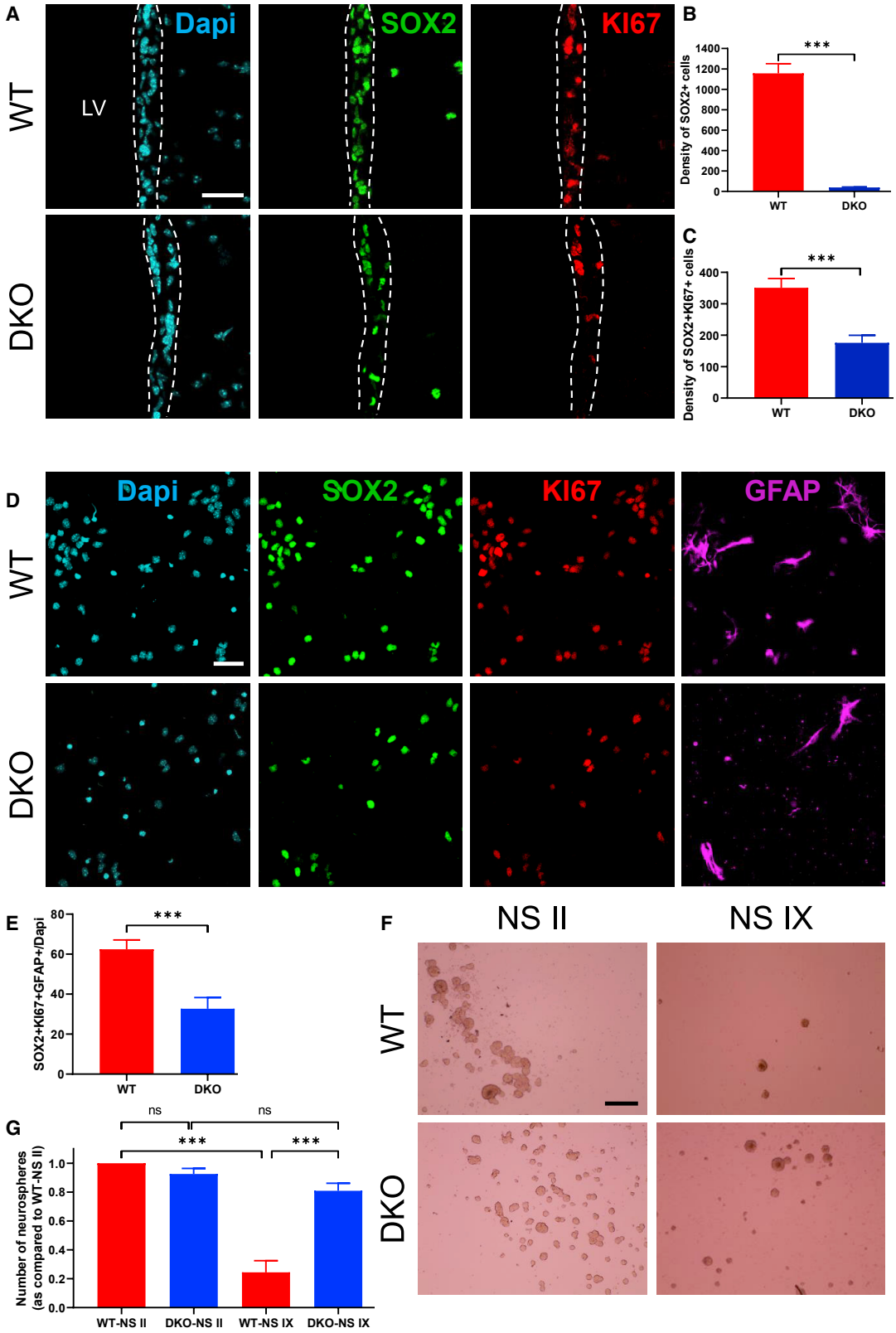

(legend on next page)

determined after 3 days *in vitro* without EGF and FGF by measuring radial migration away from adherent neurospheres (Figure 4E, left box). For this, we measured the distance of each cell that migrated from the neurosphere, and averaged the distances per neurosphere. We found that, on average, cells migrated from DKO neurospheres covered a significantly shorter distance than those migrated from WT neurospheres (WT, 259.9 ± 21.79; DKO, 181.4 ± 22.21; Mann-Whitney test, p = 0.03, U = 2; Figure 4F). Thus, ablation of *Mct8* and *Oatp1c1* reduces the migration of neurosphere-derived NPCs.

Given that the absence of THTs strongly affects SVZ neurogenesis, we investigated potential effects on olfactory behavior by performing the short-term olfactory memory test (as described in Lazarini et al., 2009). WT versus DKO mice were exposed four times to the same non-social odor (almond, lemon, or orange blossom) at different intervals (2 min, 30 min, and 1 h). We observed that the decrease in the sniffing duration of the cotton swab after two consecutive exposures to a same odor was comparable between DKO and WT mice (habituation: WT 0.46 ± 0.04; DKO 0.55 ± 0.03. Bonferroni's test following two-way ANOVA: WT $p < 0.0001$, $t = 10.15$, DKO $p < 0.0001$, $t = 10.95$; WT versus DKO $p = 0.46$, $t = 1.59$; Figure 4G), suggesting that DKO mice are able to discriminate simple odors. In contrast, after a longer interval of 30 min and 1 h, DKO mice spent significantly more time investigating the odor compared with control animals (memory, 30 min: WT, 0.28 ± 0.03; DKO, 0.82 ± 0.04. Memory, 1 h: WT, 0.16 ± 0.05; DKO, 0.97 ± 0.05; WT versus DKO. Memory 30 min, $p < 0.0001$, $t = 9.61$; memory 1 h, $p < 0.0001$, $t = 14.46$; Figure 4G). Interestingly, the investigation time of DKO mice during the last presentation (after an interval of 1 h) was not statistically different from that of the first presentation of the odor (Bonferroni's test: WT $p < 0.0001$, $t = 15.76$; DKO $p > 0.99$, $t = 0.81$). This suggests that DKO mice are unable to memorize odors. Thus, our findings show that short-term olfactory memory is affected by the absence of THTs, associating reduced adult SVZ neurogenesis with altered olfactory memory.

The Absence of MCT8 and OATP1C1 Does Not Affect SVZ Oligodendrogenesis

Lastly, we investigated whether the generation of new SVZ-OPCs was affected in DKO mice by performing an IHC for the oligodendroglia lineage markers OLIG2 and SOX10 (Figure 5A). We observed that neither the OLIG2+ nor the SOX10+ SVZ-OPC density was affected in DKO mice as compared with control animals (OLIG2: WT, 0.33 ± 0.04 cells/mm^2; DKO, 0.22 ± 0.03 cells/mm^2; Mann-Whitney test, p = 0.098, U = 24.5; Figure 5B. SOX10: WT, 0.64 ± 0.1; DKO, 0.76 ± 0.12; Mann-Whitney test, p = 0.41, U = 34.5; Figure 5C), suggesting that the generation of OPCs derived from adult SVZ-NSCs is not affected by the absence of both MCT8 and OATP1C1.

Two distinct populations of OPCs are present in the adult mammalian brain. Contrary to SVZ-OPCs that are continuously generated from NSCs in the adult SVZ, another source of oligodendrocytes is located in the parenchyma (pOPCs), notably in the corpus callosum. Since these parenchymal resident pOPCs are generated earlier during development and remain quiescent in the adult under steady-state conditions, we hypothesized that pOPCs were affected during development of DKO mice (Figure 5D). Although the SVZ area of DKO mice is unchanged compared with control SVZ (data not shown), the corpus callosum area is significantly thinner in DKO than in controls (619 ± 17.24 mm^2 in DKO mice versus 838.01 ± 53.01 mm^2 in WT), as previously observed in Mayerl et al. (2014). Using IHC, we found that the density of either OLIG2+ or SOX10+ pOPCs was strongly reduced in DKO mice as compared with WT mice (OLIG2: WT, 32.64 ± 3.05; DKO, 12.95 ± 1.05; t test, $p < 0.0001$, $t = 5.96$, df = 31; Figure 5E. SOX10: WT, 17.96 ± 1.7; DKO, 7.31 ± 0.78; t test, $p < 0.0001$, $t = 5.57$, df = 31; Figure 5F). These findings show that pOPCs are highly sensitive to the absence of

Figure 3. DKO Adult Mice Differentially Affect NSC and Progenitor Proliferation within the Lateral SVZ

(A) Representative images of proliferative NSCs (Sox2+KI67+) within the lateral SVZ from WT and DKO adult male mice. Less proliferative NSCs are observable in DKO mice.

(B and C) Statistical analysis revealed significantly decreased SOX2+ NSCs (B) and SOX2+KI67+ proliferative NSCs (C) in the lateral SVZ of DKO mice as compared with WT mice (n = 3 mice per group and n = 2–5 sections per mouse, t test, ***p < 0.001).

(D) Representative images of proliferative NSCs (SOX2+KI67+GFAP+) after plating primary neurospheres following a 24-h period under a low growth factor condition. DKO mice show less proliferative NSCs.

(E) DKO mice display a significant decreased SOX2+KI67+GFAP+ proliferative NSCs as compared with WT mice (n = 3–5 mice per group and n = 30 images per condition, Mann-Whitney test, ***p < 0.001).

(F) Representative images of floating NS II and NS IX derived from lateral SVZ of adult male WT and DKO mice.

(G) The neurosphere formation in WT mice significantly decreased after nine passages (NS IX), whereas the number of neurospheres is maintained in DKO mice (n = 3 wells per condition, two-way ANOVA followed by Bonferroni's test, ***p < 0.0001). Bars represent mean ± SEM. Scale bars: 30 μm (A and D) and 250 μm (F). LV, lateral ventricle.

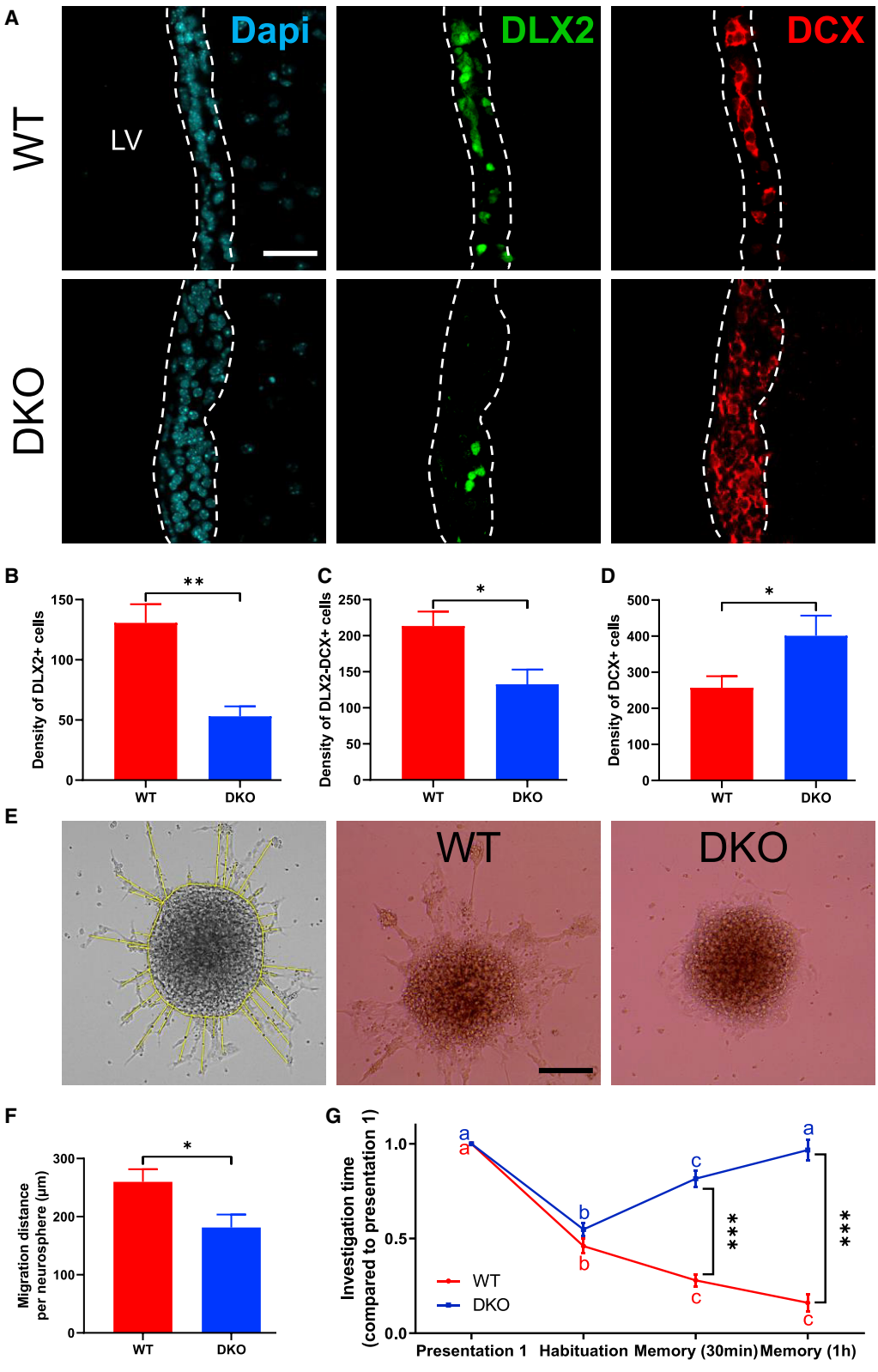

(legend on next page)

MCT8 and/or OATP1C1, whereas newly generated SVZ-OPCs are unaffected.

DISCUSSION

The SVZ niche is a well-established TH target tissue: TH preferentially drives SVZ-derived NSC fate toward a neuronal fate (Gothié et al., 2017b; López-Juárez et al., 2012; Remaud et al., 2017). In contrast, a T_3-free window due to the presence of *Dio3* and the absence of TRα1 is required for OPC generation. However, how intracellular TH levels are regulated within the different SVZ cell types remains unknown. In this study, we determined how the different components of the TH signaling pathway are modulated during NSC determination to a neuronal fate. In particular, we provide new insights into the functional role of two key THTs, MCT8 and OATP1C1, in NSC fate choice to a neuronal or a glial progenitor within the adult mouse brain. Our work shows that cellular uptake/efflux of TH through membrane transporters is involved in NSC function, affecting the generation of new neuronal and glial cells within the adult mouse brain.

Stem Cell TH Status

Our data support a key role for MCT8 and/or OATP1C1 in NSC function. First, we observed by RT-qPCR and IHC that both THTs MCT8 and OATP1C1 are highly expressed in NSCs within the adult SVZ. Second, in adult DKO mice, the density of SOX2+ NSCs and progenitors is decreased. This result was confirmed *in vitro*: the number of cycling SOX2+GFAP+ NSCs was reduced when neurospheres were grown from NSC dissected from the SVZ of DKO mice, suggesting altered stem/progenitor cell behavior in absence of THTs. Further, using the neurosphere assay, we determined that the absence of THTs does not exhaust SVZ-NSC self-renewal after IX passages, contrary to WT NSCs.

Two subpopulations of NSCs co-exist in the adult SVZ: highly proliferative stem cells (activated NSCs,aNSC) and quiescent NSCs (qNSCs) (Codega et al., 2014; Morshead et al., 1994). The mechanisms regulating the transition from a quiescent to an activated state are still poorly understood. The TH signaling pathway could be a key regulator of this cell transition, especially by controlling exit of NSCs from quiescence. The 2-fold depletion of cycling NSCs in DKO mice could indicate a return to quiescence in the absence of intracellular T_3 signaling. qNSCs contribute to the generation of neurospheres when the pool of aNSCs has been experimentally depleted (Morshead et al., 1994). Hence, the challenging *in vitro* environment could reactivate the expected accumulation of qNSCs due to the absence of functional TH signaling in DKO mice. In the absence of intracellular T_3, reactivated NSCs could proliferate indefinitely, thus maintaining the neurosphere-forming potential that we still observed after passage IX. Similarly, in the SGZ of the hippocampus, Mayerl et al. (2020) have recently demonstrated that activation of NSCs is impaired in a global *Mct8* KO adult mouse model. Furthermore, Mayerl et al. (2018) have shown that the activation of muscle stem cells is reduced to about 50% in DKO mice, impairing the myogenic program. They also found that a higher expression of both *Mct8* and *Oatp1c1* is associated with the activation of quiescent satellite stem cells. These data support our hypothesis that the absence of both THTs and intracellular T_3 induces the transition of SVZ-NSCs to a quiescent state. Altogether, our work, combined with Mayerl et al.'s studies, underlines a crucial function of MCT8 and/or OATP1C1 transporters in stem cell quiescence and reactivation. However, the relative contribution of MCT8 and/or OATP1C1 to maintain NSC

Figure 4. DKO Adult Mice Display Reduced SVZ-Derived NPCs and Impaired Neuroblast Migration within the SVZ

(A) Representative images of NPCs (DLX2+) and neuroblasts (DCX+) within the lateral SVZ from WT and DKO adult male mice.

(B–D) Quantification of uncommitted (DLX2+ cells) and committed (DLX2+DCX+ cells) neural progenitors and mature neuroblasts (DCX+ cells) within the lateral SVZ of WT and DKO male mice. DKO mice display reduced density of uncommitted (B) and committed (C) neural progenitors as compared with WT mice. In contrast, the density of mature neuroblasts (D) increased in DKO mice as compared with WT mice (n = 3 mice per group and n = 2–5 sections per mouse, t test, *p < 0.05, **p < 0.01).

(E) Representative images of the migration calculation method. Migrating cells can be seen as mixed cell outgrowth constituted by both individual and chain cells that migrate from neurospheres. The migration distance is determined using a line-drawing tool under Fiji software. The lines are drawn from the outline of the neurospheres to the center of the migrating cells. All cells that migrate from the neurospheres are considered. The two other images represent plated SVZ neurospheres generated from WT and DKO mice following a 3-day period under a low growth factor condition.

(F) *In vitro* measurement of neural precursor migration away from plated primary neurospheres shows reduced migration distance per neurosphere in DKO mice (n = 5 neurospheres per condition, Mann-Whitney test, *p < 0.05).

(G) Short-term olfactory memory behavioral test. The graph represents the time spent by WT and DKO mice to investigate the odor during the first presentation, the habituation phase (2-min later), and the two-memory phase (after 30-min and 1-h rest period). The short-term olfactory memory is impaired in DKO mice, as shown by the increase of the investigation time 30 min and 1 h after the first exposure (n = 3–5 mice per group, n = 3 experiments, two-way ANOVA followed by Bonferroni's multiple comparisons test to compare the four presentations and to compared WT and DKO mice, ***p < 0.001). Bars represent mean ± SEM. Scale bars: 30 μm (A) and 250 μm (E).

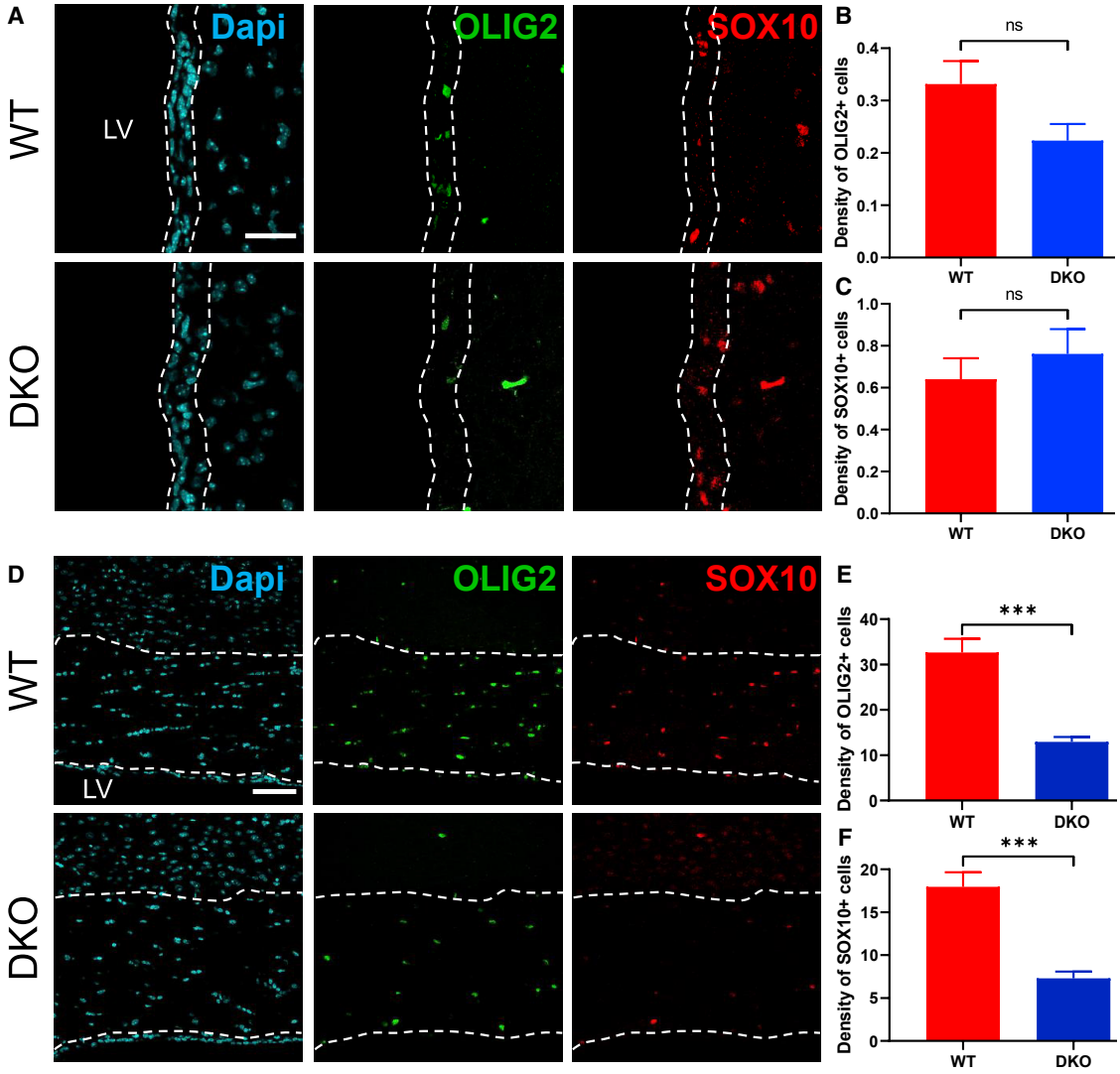

Figure 5. DKO Adult Mice Display Reduced SVZ-Derived OPCs within the Corpus Callosum but not within the SVZ

(A) Representative images of OPCs (OLIG2+ and SOX10+) within the lateral SVZ from WT and DKO adult male mice.

(B and C) Quantification of OLIG2+ (B) and SOX10+ (C) OPCs into the lateral SVZ demonstrate no density difference between WT and DKO mice (n = 3 mice per group and n = 2–5 sections per mouse, Mann-Whitney test, $p > 0.05$ non-significant).

(D) Representative images of OPCs (OLIG2+ and SOX10+) within the corpus callosum from WT and DKO adult male mice.

(E and F) DKO mice display a significant decreased OLIG2+ (E) and SOX10+ (F) OPCs density in the corpus callosum as compared with WT mice (n = 3 mice per group and n = 2–5 sections per mouse, t test, ***$p < 0.001$). Bars represent mean ± SEM. Scale bars: 30 μm (A) and 60 μm (D).

identity could be further assessed by analyzing NSC behavior in simple KO mice or following inhibition using commercially available inhibitors (Mayerl et al., 2020).

Furthermore, our *in vitro* experiments were done in the presence of T_3 (0.3 nM, present in the B27 supplement), and, in this experimental condition, we still observed a reduction in the numbers of NSCs and also impaired cell migration. Therefore, these results strongly suggest that alterations in NSCs behavior observed *in vivo* could be largely due to a local intracellular hypothyroidism. However, we cannot exclude an additional impact due to (1) the lack of MCT8 in both choroid plexus and endothelial cells of the BBB (Dumitrescu et al., 2006; Heuer et al., 2005; Trajkovic et al., 2007b) and (2) OATP1C1 facilitating T_4 uptake across the BBB and/or the CSF (Roberts et al., 2008; Mayerl et al., 2014). Furthermore, since MCT8 and OATP1C1 are also found in radial glia cells in the prenatal human brain (López-Espíndola et al., 2019), we cannot rule out a

developmental impact of the absence of both transporters contributing to the adult phenotype that we observed in the SVZ of DKO mice. Further analysis is needed to assess whether a reduction of TH availability within radial glial cells of the mouse prenatal brain has a long-lasting influence on NSC proliferation and cell fate in the adult SVZ.

A decrease of intracellular T_3 could preserve/maintain the NSC pool that can be reactivated under more favorable environmental conditions. We previously demonstrated that SVZ-NSCs are blocked in G2 phase, the phase before mitosis, following an adult-onset hypothyroidism (Lemkine et al., 2005). In the *Drosophila* brain, G2-quiescent cells are capable of reactivating faster than G0-stem cells (Otsuki and Brand, 2018). Interestingly, the localization of NSCs in their niche (i.e., dorsal versus ventral) would determine whether they enter in phase G0 or G2: under the control of patterning factors, dorsal NSCs enter G0 quiescence while ventral NSCs undergo G2 quiescence (Otsuki and Brand, 2019). Elucidating whether SVZ-NSCs are preferentially arrested either in G0 or G2 phase following a decrease of TH availability could help to adapt therapeutic purposes so as to manipulate NSC physiology and promote generation of new neural cells.

We cannot exclude that the decreased density of cycling NSCs/progenitors might be related to a developmental issue. THs are crucial for brain development: congenital hypothyroidism and AHDS (*Mct8* deficiency) are two pathological conditions where low brain TH content incurs intellectual disability (López-Espíndola et al., 2014; Schwartz and Stevenson, 2007; Vatine et al., 2017). Here, we showed that NSCs express high levels of several components of the TH signaling pathway in mice.

We speculate that high intracellular T_3 levels in NSCs (high expression of both *THTs*, *Thra1*, *Klf9*) could be acquired during the transition from embryonic/post-natal NSCs to adult NSCs. The absence of both THTs could prevent sufficient uptake of THs and therefore an intracellular lack of TH to determine the features of adult NSCs, consequently decreasing the density of proliferating NSCs, as we observed in the adult SVZ of DKO mice. Further investigation is necessary to determine whether T_3 is a key molecular signal controlling the transition from qNSC to aNSC and inversely.

Once activated, NSCs express the epidermal growth factor receptor (*Egfr*), a key proliferation-activating factor that also regulates NSC fate by blocking neurogenesis and promoting glial fate (Ayuso-Sacido et al., 2010). Interestingly, high *Egfr* expression in activated NSCs and their progeny (TACs) associates with reduced intracellular TH levels due to high expression of *Dio3* and absence of TRα1 expression (Remaud et al., 2017). Similarly, we detected a low mRNA expression of both *Mct8* and *Oatp1c1* and other THTs such as *Mct10*, *Lat1*, and *Lat2* in TACs, suggesting that absence of THTs and *TRα1*, combined with elevated *Dio3* expression (Remaud et al., 2017), is associated with actively proliferating progenitors derived from SVZ-NSCs.

MCT8 and/or OATP1C1 Absence Impairs SVZ Neurogenesis

We demonstrated that the absence of MCT8 and/or OATP1C1 impairs SVZ neurogenesis, whereas the generation of new SVZ-OPCs is unaffected. This is consistent with our previous studies showing that TH signaling acts as a neurogenic switch in SVZ-progenitors (Gothié et al., 2017b; López-Juárez et al., 2012), whereas a T_3-free window is necessary to promote SVZ oligodendrogenesis (Remaud et al., 2017). However, we did not expect to observe an accumulation of DCX+ neuroblasts along the lateral ventricles of DKO mice, suggesting a potential migration failure. Similarly, radial migration of newly generated SVZ-neural precursors was impaired *in vitro*.

Thus, the absence of MCT8 and/or OATP1C1 could alter the molecular and cellular machinery necessary for the phosphorylation of Doublecortin and the migration of neuroblasts, inducing the accumulation of newly immature neurons along the lateral ventricles. The role of TH signaling on neuroblast migration through the rostral migratory stream (RMS) remains unknown, although the role of TH in optimal cell migration has been shown in other brain regions, notably during development in the cerebellum (Morte et al., 2002; Portella et al., 2010) and neocortex (Pathak et al., 2010). Misregulation of two well-established TH target genes involved in neural migration, *reelin* (Alvarez-Dolado et al., 1999) and NCAM (Iglesias et al., 1996), blocked radial neuroblast migration, resulting in loss of cortical layering and behavioral defects. Similarly, depletion of key components of the Reelin pathway (as ApoER2/VLDLR or Dab1) resulted in accumulation of neuroblasts within the adult SVZ (Andrade et al., 2007), phenocopying the results found in our DKO mice. Thus, the interaction of TH with the Reelin signaling pathway deserves further analysis in the context of adult SVZ neurogenesis.

Using RT-qPCR analysis on isolated cell types by FACS, we observed that both *Mct8* and *Oatp1c1* mRNA were expressed at low levels in young and mature neuroblasts. In contrast, IHC allowed us to detect high expression of both MCT8 and OATP1C1 proteins in these cell types. To our knowledge, this is the first study highlighting a functional role of these transporters in the neuronal lineage derived from adult SVZ-NSCs. However, further work is needed to analyze the relative contribution of MCT8 and OATP1C1 during lineage progression of neural progenitors in the SVZ of adult mice. Recently, using similar approaches, Mayerl et al. (2020) detected high levels of

MCT8 in neuroblasts located within the hippocampus at both the mRNA and protein levels. Furthermore, they demonstrated that the density of differentiated neuroblasts is decreased in *Mct8* KO animals, showing that a global inactivation of MCT8 impaired adult neurogenesis in the mouse SGZ too. However, they found that the density of TACs and proliferating neuroblasts is unchanged in *Mct8* KO, strongly suggesting that MCT8 acts at later stages during SGZ-NSC lineage progression, during cell transition from neuroblast to immature neurons. This is consistent with previous work by Kapoor et al. (2012) showing that TH signaling targets predominantly post-mitotic committed neural progenitors and that THs accelerate neuronal differentiation both *in vivo* and *in vitro*.

These studies demonstrate that TH action on adult neurogenesis is NSC niche specific and depends on the developmental window. Contrary to the adult SGZ, our study shows that MCT8 and/or OATP1C1 are involved in the proliferation of SOX2+ TACs and DLX2+ young neuroblasts, indicating that THT-dependent TH availability regulates lineage progression at multiple steps, from NSC/progenitor proliferation (Lemkine et al., 2005) to cell-fate determination to a neuronal fate (Gothié et al., 2017b; López-Juárez et al., 2012; Remaud et al., 2017) in the adult SVZ. Our findings echo a recent study showing that MCT8 knockdown reduced the pool of progenitors and impaired neurogenesis in the chicken optic tectum, thus demonstrating that MCT8-dependent TH supply is crucial for early corticogenesis (Vancamp et al., 2017).

Compared with *Mct8* and *Oatp1c1* mRNA, mRNA levels for other THTs (*Mct10* and *Lat2*) are higher in the neuronal lineage. Further analysis is needed to study the function of these secondary THTs, *Lat2* and *Mct10*, during neuronal lineage progression. In contrast to the SVZ, Mayerl et al. (2020) detected high expression of *Mct10* (and *Mct8*, as mentioned before) in SGZ-neuroblasts, whereas *Lat1* and *Lat2* are expressed in NSCs and TACs, showing distinct expression patterns of these THTs in the two neurogenic niches. This recent finding is consistent with many others showing a complementary distribution pattern of both *Mct8* and *Mct10* in several brain areas, such as in the cerebral cortex (Müller and Heuer, 2014), strongly suggesting a compensatory function of *Mct10* in the absence of *Mct8*. Due to the mutually exclusive distribution of *Mct8* and *Mct10* mRNA in the SVZ, this neurogenic region can provide a key model to assess the physiological significance of *Mct10* as a specific THT in SVZ-derived neuroblasts. Moreover, the contribution of all these THTs to SVZ oligodendrogenesis should also be addressed. In particular, a high *Mct10* signal has been observed in white matter regions of the adult mouse brain (Müller and Heuer, 2014), raising the question of whether *Mct10* provides TH during migration of SVZ-derived oligodendrocytes toward the corpus callosum, thereby participating in axonal myelination in physiological or demyelinated conditions (Menn et al., 2006).

Thus, analyzing the function of the dynamic expression pattern of *Mct8/Oatp1c1* and other THTs in the different SVZ cell populations will open new avenues on how cell-autonomous function of the TH signaling could regulate NSC commitment to a neuronal fate.

Olfactory Function Is Affected by the Absence of Both MCT8 and OATP1C1

In rodents, newly generated neuroblasts derived from NSCs migrate through the RMS to the OBs, where they differentiate into mature interneurons throughout life. This continuous integration of new neurons into the pre-existing neuronal circuits has been implicated in olfactory behavior, including odor memory and discrimination.

We showed a decreased generation of new migrating neuroblasts in DKO mice that, together with a neuroblast migration defect, may affect the recruitment of new neurons in the adult OBs. Newly generated neurons in the olfactory network play a key role in short-term olfactory memory (Breton-Provencher et al., 2009). In particular, reduced levels of SVZ neurogenesis following antimitotic drug AraC treatment caused a depletion of SVZ cells derived from proliferating cells (Doetsch et al., 1999). Moreover, a loss of olfactory memory is observed, without affecting odor discrimination. Similarly, an upregulation of SVZ neurogenesis by an olfactory-enriched environment increased olfactory memory (Rochefort et al., 2002). These data strongly suggest that olfactory memory is dependent on the rate of adult SVZ neurogenesis and that newly generated neurons play a crucial role in establishing short-term olfactory memory, but not odor discrimination (Breton-Provencher et al., 2009; Enwere et al., 2004). Finally, absence of MCT8 and/or OATP1C1 impairs (1) generation and migration of SVZ-neuroblasts, and (2) olfactory capacities, suggesting that SVZ neurogenesis in DKO mice is functionally impaired. However, the discriminative capacity of WT and DKO mice was tested using simple, easily discernable odors. Some studies have previously demonstrated that discrimination between two simple different odors is not impaired in mice with reduced SVZ neurogenesis (Breton-Provencher et al., 2009; Enwere et al., 2004). We cannot rule out that more difficult discrimination tasks using very similar odorants would have been more challenging for DKO mice, as it has been recently demonstrated in other mouse models aiming to analyze the impact of aging (Enwere et al., 2004) and consequences of a transitory increase of the NSC pool on olfactory discrimination (Bragado Alonso et al., 2019).

Myelination Status

TH deficiency is usually linked to impaired myelogenesis during development. It is well established that TH controls the timing of oligodendrocyte differentiation (Barres et al., 1994; Billon et al., 2002; Kim and Petratos, 2019). Our work showed that DKO mice have a significant lower density of resident pOPCs localized in the corpus callosum, above the lateral ventricle, corresponding to the reduced myelination observed in the corpus callosum of DKO brains with a silver staining technique (Mayerl et al., 2014). This hypomyelination state is associated with neurological and behavioral impairments described in DKO mice as well as in AHDS patients (Mayerl et al., 2014). Postmortem brain tissue analysis of an AHDS patient strongly suggest that MCT8 drives T_3-dependent differentiation of OPC into mature and functional myelinating oligodendrocytes (López-Espíndola et al., 2014). These resident pOPCs, widely distributed in the parenchyma throughout the adult brain, are generated during development and can remain quiescent throughout adult life (Tokumoto et al., 2017). The significant reduction of resident parenchymal pOPCs in the corpus callosum could reflect neurodevelopmental and behavioral consequences of *Mct8* and *Oatp1c1* depletion in the developmental DKO mouse model. A conditional DKO mouse line would permit researchers to better distinguish effects generated early during development from those affected later during adulthood. Lastly, the crucial role of MCT8 in the differentiation of OPCs is known in humans: MCT8 downregulation in human embryonic stem cell-derived cells induces oligodendrocyte apoptosis and myelin damage (Lee et al., 2017). These data suggest that the decrease in resident OPCs in the corpus callosum of DKO mice could be due to OPCs apoptosis.

In contrast to resident pOPCs, our work shows that newly generated OPCs derived from adult SVZ-NSCs express neither MCT8 nor OATP1C1, with generation of new OPCs in the SVZ of DKO mice being unaffected. Our previous results showed that a transient hypothyroidism promotes the generation of new SVZ-OPCs and not resident pOPCs, demonstrating that both OPC populations differentially respond to a TH-free window (Gothié et al., 2017a; Remaud et al., 2017). The discrepancy observed in the number of the SVZ-OPCs compared with our previously published data could depend on the timing of when hypothyroidism was induced. In Remaud et al. (2017) and Gothié et al. (2017a), we induced a systemic transient hypothyroidism in adult mice, whereas, in the present work, brain TH deficiency already occurs during developmental stages. Thus, the absence of an increase in OPCs in the DKO mice could be due to a developmental defect. Several studies underline that SVZ-OPCs are more capable of functional repair in demyelinating lesions than pOPCs (Brousse et al., 2015; Remaud et al., 2017; Xing et al., 2014). Thus, how TH signaling preferentially regulates SVZ-OPCs, an efficient source of remyelinating cells, will provide new therapeutic options to favor myelin repair in multiple sclerosis and other demyelinating diseases. More precisely, understanding how local intracellular TH levels differentially regulate SVZ-OPCs and resident OPCs could overcome the gap of knowledge on the distinct behavior of these two kinds of OPCs after a myelin insult.

Conclusion

This work highlights, first, a new role of MCT8 and/or OATP1C1 in adult NSC physiology; second, a tight and dynamic regulation of TH signaling during neuronal lineage progression; and third, an impairment of olfactory behavior and memory. Our data could shed new light on potential therapeutic purposes for AHDS patients and more generally for demyelinating diseases where new remyelinating cells are needed. The neurological phenotype of DKO mice and AHDS patients could be due to a developmental defect worsened by an impaired neurogenesis in the adult.

EXPERIMENTAL PROCEDURES

Animals

Generation and genotyping of Mct8 KO and *Mct8/Oatp1c1* DKO male mice were reported elsewhere (Mayerl et al., 2014; Trajkovic et al., 2007b). For visualizing OATP1C1-expressing cells, transgenic animals were used that express YFP reporter and a tamoxifen-inducible cre-recombinase under the control of the *Slco1c1* promoter (Ridder et al., 2011). Four weeks prior to immunofluorescence analysis, these OATP1C1:YFP reporter mice were treated with tamoxifen (40 μg/g intraperitoneally) for five consecutive days in order to induce YFP expression specifically in OATP1C1 expressing cells.

Only male mice on a C57BL/6 background at the age of 2 months (WT, DKO; OATP1C1:YFP) or 4 months (*Mct8* KO) were used in the study. *Mct8* KO, DKO, OATP1C1:YFP mice, and age-matched WT mice on the same genetic background were obtained from the Heuer lab. C57BL/6 WT mice purchased from Janvier Labs (Le Genest St. Isle, France) were used for the qRT-PCR experiment (see protocols below). Mice were left undisturbed for at least 10 days after arrival in the animal facility to limit environmental stress due to transport and to allow a better acclimatization to their new environment. Mice were housed with an enriched environment to ameliorate anxious behavior. Mice were kept under standard conditions (22°C, 50% humidity, 12 h light/dark cycle) and food and water were available *ad libitum*. Animals were handled and cared for in accordance with the EU directive of 22 September 2010 (2010/63/EU). All procedures were conducted according to the principles and procedures in Guidelines for Care and Use of Laboratory Animals and validated by local and national ethical committees (CEEA, comité d'ethique en expérimentation animale, Cuvier

n°68; AZ 84-02.04.2017.A219 LANUV NRW Recklinghausen Germany).

Olfactory Function

The procedure is described in the Supplemental Information.

Tissue Preparation and IHC

Three WT and three DKO mice were anesthetized with pentobarbital (130 mg/kg, Centravet) and perfused rapidly through the left heart ventricle with 1× PBS followed by 4% paraformaldehyde in PBS (0.1 M, pH 7.4). Brains were harvested and post fixed at 4°C in the same fixative solution overnight. Brains were cryoprotected in 30% sucrose in 1× PBS at 4°C and embedded in OCT, optimal cutting temperature compound (Sakura) and stored at −80°C. Brain coronal sections (30 μm thick) were performed using a cryostat and were rigorously selected from bregma +0.9 mm to −0.1 mm and then collected in sterile 1× PBS. The IHC procedure is described in the Supplemental Information.

Imaging and Quantification

A Leica TCS-SP5 confocal microscope was used to acquire fluorescence images (1,024 × 1,024 pixels; 400× magnification). Images were taken on 3–5 sections per mouse. Three detailed images were taken lining the lateral ventricles corresponding to the lateral SVZ of both sides to quantify NSCs, NPCs, and OPCs. In addition, three images were taken of the corpus callosum at each side to quantify the density of pOPCs. Cell counting was performed in the freely available Fiji software. For each image, the region of interest (i.e., the lateral ventricular border or the corpus callosum) was drawn. Moreover, the immunopositive cells were quantified using the cell counter plugin. The results were expressed as the number of immunopositive cells per mm^2. For MCT8 and OATP1C1 colocalization with the plasma membrane marker pan-cadherin, z stack images were acquired using 1,024 × 1,024 pixels; stack images, 0.34 μm; 630× magnification zoom, 2.5; visualizations were done on Max Intensity Z projections using Fiji software; and 3D reconstitution were processed using Imaris software.

Adult Neurosphere Assay

Three WT and five DKO animals were sacrificed by cervical dislocation and the region containing the lateral SVZ was dissected. Tissues were incubated in digestion medium (papain [Worthington], DNase [Worthington], L-cysteine [Sigma-Aldrich]) for 30 min at 37°C and mechanically dissociated to obtain a single-cell suspension. Cells were collected by centrifugation at 1,000 rcf (relative centrifugal force) for 5 min and then cultured in a tissue culture flask 25 (Techno Plastic Products, TPP) containing DMEM-F12 (Gibco), 40 mg/mL insulin (Sigma), 1/200 B-27 supplement (Gibco) containing 0.3 nM T_3, 1/100 N-2 supplement (Gibco), 0.3% glucose (Sigma-Aldrich), 5 nM HEPES (Thermo Fisher), 100 U/mL penicillin/streptomycin (Thermo Fisher), 20 ng/mL EGF (Peprotech), and 20 ng/mL FGF2 (Peprotech) to obtain primary neurospheres. The cultures were maintained in a 5% CO_2 environment at 37°C for 7 days and the growing medium was supplemented with EGF and FGF2 every 2 days.

Primary neurospheres were first used for cell migration (procedure described in the Supplemental Information). To analyze cell differentiation, primary neurospheres were dissociated and 50 × 10^3 cells were plated in eight-well glass slides (PEZGS0816, Millicell) coated with poly-D-lysine (0.1 mg/mL, Sigma-Aldrich). Differentiation was induced by EGF and FGF2 withdrawal. After 24 h of differentiation, cells were fixed with 4% paraformaldehyde in PBS (0.1 M, pH 7.4). IHC was performed as described above. Quantifications were done on maximum intensity Z projections of 4-μm stack images using Fiji software. Results are presented as the number of immunopositive cells with respect to the total number of cells.

Clonality Neurosphere Assay

Primary neurospheres (NS I), obtained as indicated above, were dissociated and then plated at 10,000 cells/mL concentration in 24-well tissue culture test plates (TPP) as indicated above (n = 5–10 wells per passage, n = 1 experimental replicate). Three wells of floating neurospheres (NS II to NS IX) were imaged with EVOS XL Core cell imaging system microscope (×10) and the number of neurospheres per well was determined using Fiji software.

Flow Cytometry and Real-Time PCR

Procedure is described in the Supplemental Information.

Statistical Analysis

Statistical analyses were performed with GraphPad Prism8 software (GraphPad Software, San Diego, CA) and StatXact8 (Cytel Inc.). A Kruskal-Wallis test followed by permutation test was used for the qPCR analyses. For *in vivo* and *in vitro* quantifications, means from two groups were compared using a two-tailed Student's t test or a Mann-Whitney U test, depending on whether data were normally distributed or not, respectively. A two-way ANOVA test followed by a Bonferroni post test was used to compare the number of neurospheres and the short-term olfactory memory in CTL, control and DKO mice. Differences were considered statistically significant for a p value <0.05. Data are presented in the histograms and expressed as mean ± SEM or in the boxplots with medians, minimum, and maximum values.

SUPPLEMENTAL INFORMATION

Supplemental Information can be found online at https://doi.org/10.1016/j.stemcr.2020.12.009.

AUTHOR CONTRIBUTIONS

C.L., L.B., A.S., and K.L. conducted the experiments. C.L., L.B., A.S., and K.L. did cell counting and analyzed data. M.S. and H.H., provided the transgenic mice. C.L., L.B., A.S., S.R., and B.D. designed the experiments and wrote the paper. All authors were involved in commenting on the paper.

ACKNOWLEDGMENTS

The authors would like to thank S. Sosinsky and F. Uridat for the excellent animal care. We also thank the ImagoSeine platform of the Institute Jacques Monod, Université René Descartes for the imaging advice. This work was supported by the CNRS and the EU H2020 contract Thyrage (grant n°666869). H.H. and M.S. are supported by the Deutsche Forschungsgemeinschaft (DFG; TR 296/1-P01).

Received: July 30, 2020
Revised: December 15, 2020
Accepted: December 15, 2020
Published: January 14, 2021

REFERENCES

Alvarez-Dolado, M., Ruiz, M., Del Río, J.A., Alcántara, S., Burgaya, F., Sheldon, M., Nakajima, K., Bernal, J., Howell, B.W., Curran, T., et al. (1999). Thyroid hormone regulates reelin and dab1 expression during brain development. J. Neurosci. *19*, 6979–6993.

Andrade, N., Komnenovic, V., Blake, S.M., Jossin, Y., Howell, B., Goffinet, A., Schneider, W.J., and Nimpf, J. (2007). ApoER2/VLDL receptor and Dab1 in the rostral migratory stream function in postnatal neuronal migration independently of Reelin. Proc. Natl. Acad. Sci. *104*, 8508–8513.

Astapova, I., and Hollenberg, A.N. (2013). The in vivo role of nuclear receptor corepressors in thyroid hormone action. Biochim. Biophys. Acta - Gen. Subj. *1830*, 3876–3881.

Ayuso-Sacido, A., Moliterno, J.A., Kratovac, S., Kapoor, G.S., O'Rourke, D.M., Holland, E.C., García-Verdugo, J.M., Roy, N.S., and Boockvar, J.A. (2010). Activated EGFR signaling increases proliferation, survival, and migration and blocks neuronal differentiation in post-natal neural stem cells. J. Neurooncol. *97*, 323–337.

Barres, B.A., Lazar, M.A., and Raff, M.C. (1994). A novel role for thyroid hormone, glucocorticoids and retinoic acid in timing oligodendrocyte development. Development *120*, 1097–1108.

Bianco, A.C., and Kim, B.W. (2006). Deiodinases: Implications of the local control of thyroid hormone action. J. Clin. Invest. *116*, 2571–2579.

Billon, N., Jolicoeur, C., Tokumoto, Y., Vennström, B., and Raff, M. (2002). Normal timing of oligodendrocyte development depends on thyroid hormone receptor alpha 1 (TRα1). EMBO J. *21*, 6452–6460.

Bragado Alonso, S., Reinert, J.K., Marichal, N., Massalini, S., Berninger, B., Kuner, T., and Calegari, F. (2019). An increase in neural stem cells and olfactory bulb adult neurogenesis improves discrimination of highly similar odorants. EMBO J. *38*, e98791.

Breton-Provencher, V., Lemasson, M., Peralta, M.R., and Saghatelyan, A. (2009). Interneurons produced in adulthood are required for the normal functioning of the olfactory bulb network and for the execution of selected olfactory behaviors. J. Neurosci. *29*, 15245–15257.

Brousse, B., Magalon, K., Durbec, P., and Cayre, M. (2015). Region and dynamic specificities of adult neural stem cells and oligodendrocyte precursors in myelin regeneration in the mouse brain. Biol. Open *4*, 980–992.

Codega, P., Silva-Vargas, V., Paul, A., Maldonado-Soto, A.R., DeLeo, A.M., Pastrana, E., and Doetsch, F. (2014). Prospective identification and purification of quiescent adult neural stem cells from their in vivo niche. Neuron *82*, 545–559.

Doetsch, F., García-Verdugo, J.M., and Alvarez-Buylla, A. (1999). Regeneration of a germinal layer in the adult mammalian brain. Proc. Natl. Acad. Sci. U. S. A. *96*, 11619–11624.

Dumitrescu, A.M., Liao, X.H., Best, T.B., Brockmann, K., and Refetoff, S. (2004). A novel syndrome combining thyroid and neurological abnormalities is associated with mutations in a monocarboxylate transporter Gene. Am. J. Hum. Genet. *74*, 168–175.

Dumitrescu, A.M., Liao, X.H., Weiss, R.E., Millen, K., and Refetoff, S. (2006). Tissue-specific thyroid hormone deprivation and excess in monocarboxylate transporter (Mct) 8-deficient mice. Endocrinology *147*, 4036–4043.

Enwere, E., Shingo, T., Gregg, C., Fujikawa, H., Ohta, S., and Weiss, S. (2004). Aging results in reduced epidermal growth factor receptor signaling, diminished olfactory neurogenesis, and deficits in fine olfactory discrimination. J. Neurosci. *24*, 8354–8365.

Fanibunda, S.E., Desouza, L.A., Kapoor, R., Vaidya, R.A., and Vaidya, V.A. (2018). In Thyroid Hormone Regulation of Adult Neurogenesis, G.B.T.-V. Vitam Horm and H. Litwack, eds. (Academic Press), pp. 211–251.

Flamant, F., and Gauthier, K. (2013). Thyroid hormone receptors: The challenge of elucidating isotype-specific functions and cell-specific response. Biochim. Biophys. Acta - Gen. Subj. *1830*, 3900–3907.

Friesema, E.C.H., Ganguly, S., Abdalla, A., Fox, J.E.M., Halestrap, A.P., and Visser, T.J. (2003). Identification of monocarboxylate transporter 8 as a specific thyroid hormone transporter. J. Biol. Chem. *278*, 40128–40135.

Friesema, E.C.H., Grueters, P.A., Biebermann, H., Krude, H., Von Moers, A., Reeser, M., Barrett, T.G., Mancilla, E.E., Svensson, J., Kester, M.H.A., et al. (2004). Association between mutations in a thyroid hormone transporter and severe X-linked psychomotor retardation. Lancet *364*, 1435–1437.

Gothié, J.D., Sébillot, A., Luongo, C., Legendre, M., Nguyen Van, C., Le Blay, K., Perret-Jeanneret, M., Remaud, S., and Demeneix, B.A. (2017a). Adult neural stem cell fate is determined by thyroid hormone activation of mitochondrial metabolism. Mol. Metab. *6*, 1551–1561.

Gothié, J.D., Demeneix, B., and Remaud, S. (2017b). Comparative approaches to understanding thyroid hormone regulation of neurogenesis. Mol. Cell. Endocrinol. *459*, 1041–1115.

Groeneweg, S., van Geest, F.S., Peeters, R.P., Heuer, H., and Visser, W.E. (2019). Thyroid hormone transporters. Endocr. Rev. *41*, 146–201.

Heuer, H., Maier, M.K., Iden, S., Mittag, J., Friesema, E.C.H., Visser, T.J., and Bauer, K. (2005). The monocarboxylate transporter 8 linked to human psychomotor retardation is highly expressed in thyroid hormone-sensitive neuron populations. Endocrinology *146*, 1701–1706.

Hu, F., Knoedler, J.R., and Denver, R.J. (2016). A mechanism to enhance cellular responsivity to hormone action: Krüppel-like factor 9 promotes thyroid hormone receptor-β autoinduction during postembryonic brain development. Endocrinology *157*, 1683–1693.

Iglesias, T., Caubín, J., Stunnenberg, H.G., Zaballos, A., Bernal, J., and Muñoz, A. (1996). Thyroid hormone- dependent

transcriptional repression of neural cell adhesion molecule during brain maturation. EMBO J *15*, 4307–4316.

Kim, M.J., and Petratos, S. (2019). Oligodendroglial lineage cells in thyroid hormone-deprived conditions. Stem Cells Int *2019*, 5496891.

Kapoor, R., Desouza, L.A., Nanavaty, I.N., Kernie, S.G., and Vaidya, V.A. (2012). Thyroid hormone accelerates the differentiation of adult hippocampal progenitors. J. Neuroendocrinol. *24*, 1259–1271.

Kapoor, R., Fanibunda, S.E., Desouza, L.A., Guha, S.K., and Vaidya, V.A. (2015). Perspectives on thyroid hormone action in adult neurogenesis. J. Neurochem. *133*, 599–616.

Lazarini, F., Mouthon, M.A., Gheusi, G., de Chaumont, F., Olivo-Marin, J.C., Lamarque, S., Abrous, D.N., Boussin, F.D., and Lledo, P.M. (2009). Cellular and behavioral effects of cranial irradiation of the subventricular zone in adult mice. PLoS One *4*, e7017.

Lee, J.Y., Kim, M.J., Deliyanti, D., Azari, M.F., Rossello, F., Costin, A., Ramm, G., Stanley, E.G., Elefanty, A.G., Wilkinson-Berka, J.L., et al. (2017). Overcoming monocarboxylate transporter 8 (MCT8)-deficiency to promote human oligodendrocyte differentiation and myelination. EBioMedicine *25*, 122–135.

Lemkine, G.F., Raji, A., Alfama, G., Turque, N., Hassani, Z., Alegria-Prévot, O., Samarut, J., Levi, G., and Demeneix, B.A. (2005). Adult neural stem cell cycling in vivo requires thyroid hormone and its alpha receptor. FASEB J. *19*, 863–865.

López-Espíndola, D., Morales-Bastos, C., Grijota-Martínez, C., Liao, X.H., Lev, D., Sugo, E., Verge, C.F., Refetoff, S., Bernal, J., and Guadaño-Ferraz, A. (2014). Mutations of the thyroid hormone transporter MCT8 cause prenatal brain damage and persistent hypomyelination. J. Clin. Endocrinol. Metab. *99*, E2799–E2804.

López-Espíndola, D., García-Aldea, Á., Gómez de la Riva, I., Rodríguez-García, A.M., Salvatore, D., Visser, T.J., Bernal, J., and Guadaño-Ferraz, A. (2019). Thyroid hormone availability in the human fetal brain: novel entry pathways and role of radial glia. Brain Struct. Funct. *224*, 2103–2119.

López-Juárez, A., Remaud, S., Hassani, Z., Jolivet, P., Pierre Simons, J., Sontag, T., Yoshikawa, K., Price, J., Morvan-Dubois, G., and Demeneix, B.A. (2012). Thyroid hormone signaling acts as a neurogenic switch by repressing Sox2 in the adult neural stem cell niche. Cell Stem Cell *10*, 531–543.

Luongo, C., Dentice, M., and Salvatore, D. (2019). Deiodinases and their intricate role in thyroid hormone homeostasis. Nat. Rev. Endocrinol. *15*, 479–488.

Mayerl, S., Visser, T.J., Darras, V.M., Horn, S., and Heuer, H. (2012). Impact of Oatp1c1 deficiency on thyroid hormone metabolism and action in the mouse brain. Endocrinology *153*, 1528–1537.

Mayerl, S., Müller, J., Bauer, R., Richert, S., Kassmann, C.M., Darras, V.M., Buder, K., Boelen, A., Visser, T.J., and Heuer, H. (2014). Transporters MCT8 and OATP1C1 maintain murine brain thyroid hormone homeostasis. J. Clin. Invest. *124*, 1987–1999.

Mayerl, S., Schmidt, M., Doycheva, D., Darras, V.M., Hüttner, S.S., Boelen, A., Visser, T.J., Kaether, C., Heuer, H., and von Maltzahn, J. (2018). Thyroid hormone transporters MCT8 and OATP1C1 control skeletal muscle regeneration. Stem Cell Reports *10*, 1959–1974.

Mayerl, S., Heuer, H., and Ffrench-Constant, C. (2020). Hippocampal neurogenesis requires cell-autonomous thyroid hormone signaling. Stem Cell Reports *14*, 845–860.

Menn, B., Garcia-Verdugo, J.M., Yaschine, C., Gonzalez-Perez, O., Rowitch, D., and Alvarez-Buylla, A. (2006). Origin of oligodendrocytes in the subventricular zone of the adult brain. J. Neurosci. *26*, 7907–7918.

Morshead, C.M., Reynolds, B.A., Craig, C.G., McBurney, M.W., Staines, W.A., Morassutti, D., Weiss, S., and van der Kooy, D. (1994). Neural stem cells in the adult mammalian forebrain: a relatively quiescent subpopulation of subependymal cells. Neuron *13*, 1071–1082.

Morte, B., Manzano, J., Scanlan, T., Vennström, B., and Bernal, J. (2002). Deletion of the thyroid hormone receptor alpha 1 prevents the structural alterations of the cerebellum induced by hypothyroidism. Proc. Natl. Acad. Sci. U. S. A. *99*, 3985–3989.

Müller, J., and Heuer, H. (2014). Expression pattern of thyroid hormone transporters in the postnatal mouse brain. Front. Endocrinol. *5*, 92.

Nait-Oumesmar, B., Picard-Riera, N., Kerninon, C., Decker, L., Seilhean, D., Höglinger, G.U., Hirsch, E.C., Reynolds, R., and Baron-Van Evercooren, A. (2007). Activation of the subventricular zone in multiple sclerosis: Evidence for early glial progenitors. Proc. Natl. Acad. Sci. U. S. A. *104*, 4694–4699.

Otsuki, L., and Brand, A.H. (2018). Cell cycle heterogeneity directs the timing of neural stem cell activation from quiescence. Science *360*, 99–102.

Otsuki, L., and Brand, A.H. (2019). Dorsal-ventral differences in neural stem cell quiescence are induced by p57KIP2/Dacapo. Dev. Cell *49*, 293–300.e3.

Pathak, A., Sinha, R.A., Mohan, V., Mitra, K., and Godbole, M.M. (2010). Maternal thyroid hormone before the onset of fetal thyroid function regulates reelin and downstream signaling cascade affecting neocortical neuronal migration. Cereb. Cortex *21*, 11–21.

Pizzagalli, F., Hagenbuch, B., Stieger, B., Klenk, U., Folkers, G., and Meier, P.J. (2002). Identification of a novel human organic anion transporting polypeptide as a high affinity thyroxine transporter. Mol. Endocrinol. *16*, 2283–2296.

Portella, A.C., Carvalho, F., Faustino, L., Wondisford, F.E., Ortiga-Carvalho, T.M., and Gomes, F.C.A. (2010). Thyroid hormone receptor β mutation causes severe impairment of cerebellar development. Mol. Cell. Neurosci. *44*, 68–77.

Remaud, S., Ortiz, F.C., Perret-Jeanneret, M., Aigrot, M.S., Gothié, J.D., Fekete, C., Kvárta-Papp, Z., Gereben, B., Langui, D., Lubetzki, C., et al. (2017). Transient hypothyroidism favors oligodendrocyte generation providing functional remyelination in the adult mouse brain. eLife *6*, e29996.

Ridder, D.A., Lang, M.-F., Salinin, S., Röderer, J.-P., Struss, M., Maser-Gluth, C., and Schwaninger, M. (2011). TAK1 in brain endothelial cells mediates fever and lethargy. J. Exp. Med. *208*, 2615–2623.

Roberts, L.M., Woodford, K., Zhou, M., Black, D.S., Haggerty, J.E., Tate, E.H., Grindstaff, K.K., Mengesha, W., Raman, C., and

Zerangue, N. (2008). Expression of the thyroid hormone transporters monocarboxylate transporter-8 (SLC16A2) and organic ion transporter-14 (SLCO1C1) at the blood-brain barrier. Endocrinology *149*, 6251–6261.

Rochefort, C., Gheusi, G., Vincent, J.D., and Lledo, P.M. (2002). Enriched odor exposure increases the number of newborn neurons in the adult olfactory bulb and improves odor memory. J. Neurosci. *22*, 2679–2689.

Schwartz, C.E., and Stevenson, R.E. (2007). The MCT8 thyroid hormone transporter and Allan-Herndon-Dudley syndrome. Best Pract. Res. Clin. Endocrinol. Metab. *21*, 307–321.

Strømme, P., Groeneweg, S., Lima De Souza, E.C., Zevenbergen, C., Torgersbråten, A., Holmgren, A., Gurcan, E., Meima, M.E., Peeters, R.P., Visser, W.E., et al. (2018). Mutated thyroid hormone transporter OATP1C1 associates with severe brain hypometabolism and juvenile neurodegeneration. Thyroid *28*, 1406–1415.

Suzuki, S., Mori, J., and Hashizume, K. (2007). μ-crystallin, a NADPH-dependent T3-binding protein in cytosol. Trends Endocrinol. Metab. *18*, 286–289.

Tokumoto, Y., Tamaki, S., Kabe, Y., Takubo, K., and Suematsu, M. (2017). Quiescence of adult oligodendrocyte precursor cells requires thyroid hormone and hypoxia to activate Runx1. Sci. Rep. *7*, 1019.

Trajkovic, M., Visser, T.J., Mittag, J., Horn, S., Lukas, J., Darras, V.M., Raivich, G., Bauer, K., and Heuer, H. (2007a). Abnormal thyroid hormone metabolism in mice lacking the monocarboxylate transporter 8. J. Clin. Invest. *117*, 627–635.

Trajkovic, M., Visser, T.J., Mittag, J., Horn, S., Lukas, J., Darras, V.M., Raivich, G., Bauer, K., and Heuer, H. (2007b). Abnormal thyroid hormone metabolism in mice lacking the monocarboxylate transporter 8. J. Clin. Invest. *117*, 627–635.

Vancamp, P., Deprez, M.A., Remmerie, M., and Darras, V.M. (2017). Deficiency of the thyroid hormone transporter monocarboxylate transporter 8 in neural progenitors impairs cellular processes crucial for early corticogenesis. J. Neurosci. *37*, 11616–11631.

Vancamp, P., Gothié, J.-D., Luongo, C., Sébillot, A., Le Blay, K., Butruille, L., Pagnin, M., Richardson, S.J., Demeneix, B.A., and Remaud, S. (2019). Gender-specific effects of transthyretin on neural stem cell fate in the subventricular zone of the adult mouse. Sci. Rep. *9*, 19689.

Vatine, G.D., Al-Ahmad, A., Barriga, B.K., Svendsen, S., Salim, A., Garcia, L., Garcia, V.J., Ho, R., Yucer, N., Qian, T., et al. (2017). Modeling psychomotor retardation using iPSCs from MCT8-deficient patients indicates a prominent role for the blood-brain barrier. Cell Stem Cell *20*, 831–843.e5.

Wittmann, G., Szabon, J., Mohácsik, P., Nouriel, S.S., Gereben, B., Fekete, C., and Lechan, R.M. (2015). Parallel regulation of thyroid hormone transporters OATP1c1 and MCT8 during and after endotoxemia at the blood-brain barrier of male rodents. Endocrinology *156*, 1552–1564.

Yoshioka, K., Namiki, K., Sudo, T., and Kasuya, Y. (2015). p38α controls self-renewal and fate decision of neurosphere-forming cells in adult hippocampus. FEBS Open Bio *5*, 437–444.

Xing, Y.L., Röth, P.T., Stratton, J.A.S., Chuang, B.H.A., Danne, J., Ellis, S.L., Ng, S.W., Kilpatrick, T.J., and Merson, T.D. (2014). Adult neural precursor cells from the subventricular zone contribute significantly to oligodendrocyte regeneration and remyelination. J. Neurosci. *34*, 14128–14146.

Stem Cell Reports, Volume *16*

Supplemental Information

Absence of Both Thyroid Hormone Transporters MCT8 and OATP1C1 Impairs Neural Stem Cell Fate in the Adult Mouse Subventricular Zone

Cristina Luongo, Lucile Butruille, Anthony Sébillot, Karine Le Blay, Markus Schwaninger, Heike Heuer, Barbara A. Demeneix, and Sylvie Remaud

Fig. S1

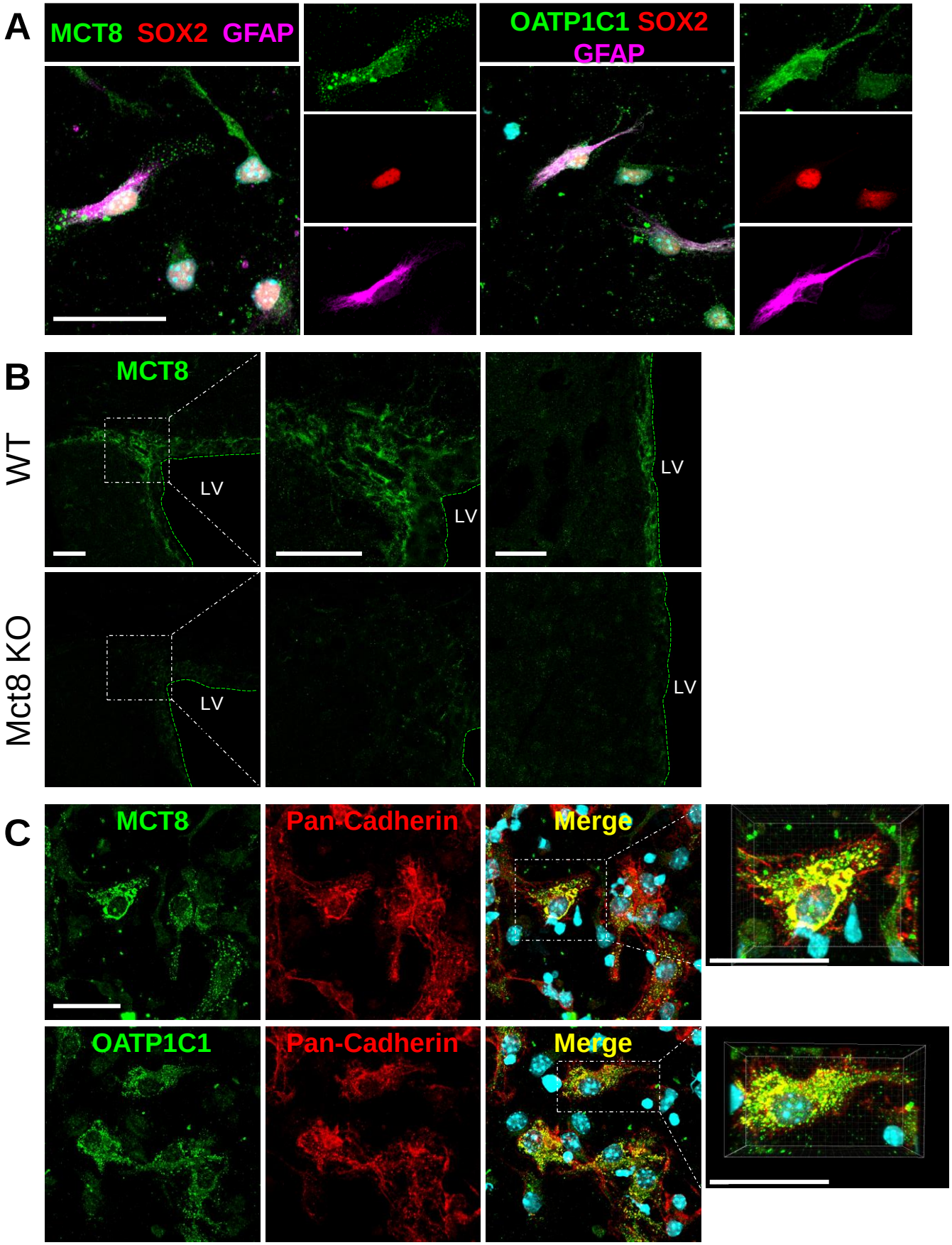
A
MCT8 SOX2 GFAP
OATP1C1 SOX2 GFAP
B
WT
Mct8 KO
MCT8
LV
C
MCT8
Pan-Cadherin
Merge
OATP1C1

Figure S1. Expression and localization of MCT8 and OATP1C1 transporters. Related to Figure 1
(A) *In vitro* expression of MCT8 and OATP1C1 THTs in single cells dissociated from neurospheres. MCT8 and OATP1C1 are strongly expressed in SOX2+ and GFAP+ NSCs. (B) Specificity of the MCT8 antibody. MCT8 is totally absent in the dorsal and lateral SVZ of Mct8 KO mice. (C) MCT8 and OATP1C1 colocalization with the plasma membrane marker pan-Cadherin. Three-D reconstruction demonstrates the *in vitro* membrane localization of both THTs. Scale bars: 30µm (A), 50µm (B) and 30µm (C).

Fig. S2

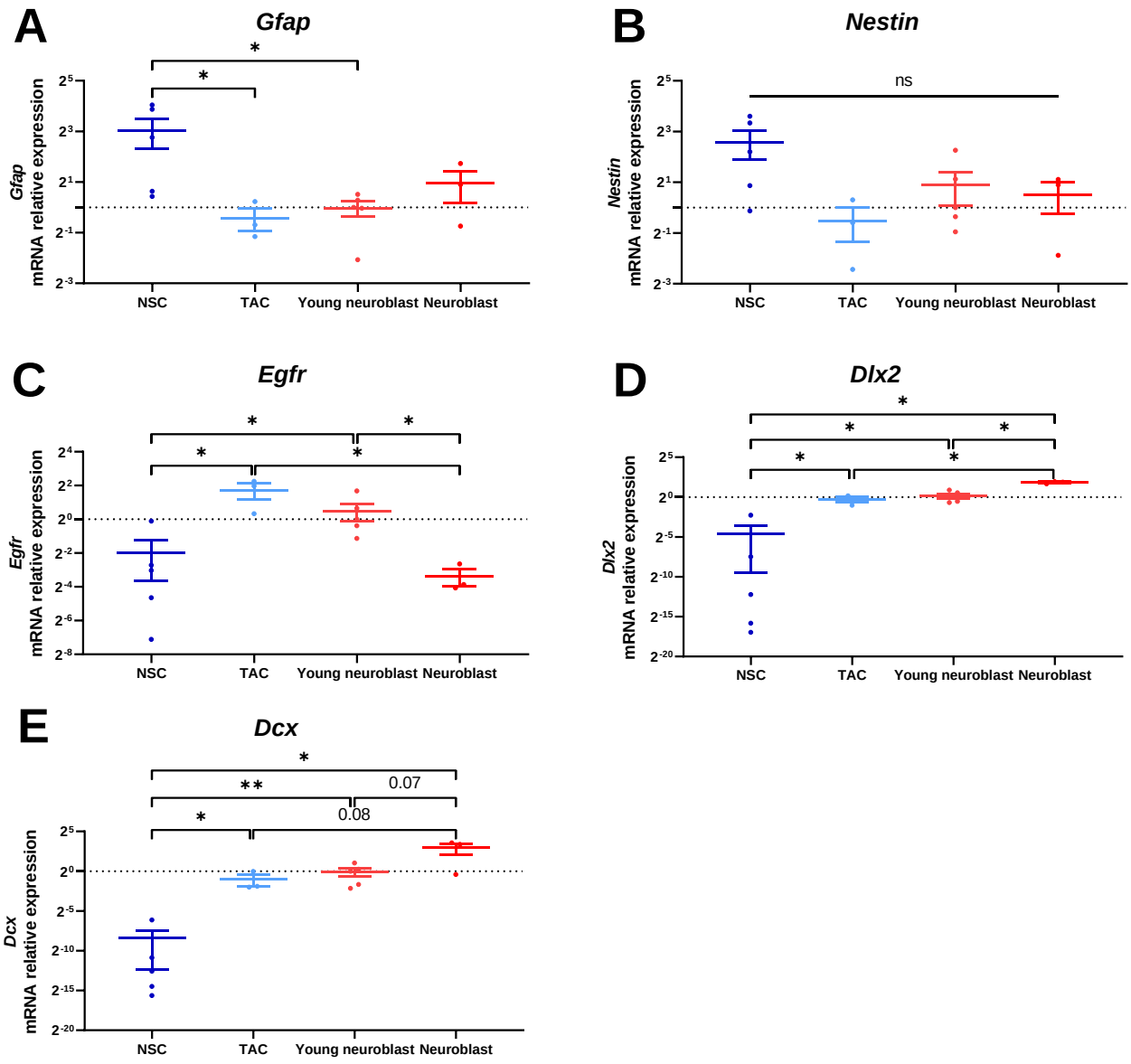
A
Gfap
Gfap mRNA relative expression
NSC
TAC
Young neuroblast
Neuroblast
B
Nestin
Nestin mRNA relative expression
ns
C
Egfr
Egfr mRNA relative expression
D
Dlx2
Dlx2 mRNA relative expression
E
Dcx
Dcx mRNA relative expression
0.07
0.08

Figures S2. Expression of cell type-specific marker genes at each stage of the neuronal lineage. Related to Figure 2

(A-B) Detection of NSCs mRNA expression levels *Gfap* (A) and *Nestin* (B) in FACS-sorted SVZ cells of five adult WT male mice. (C) Gene expression analysis of transient amplifying cells mRNA *Egfr* in SVZ. (D-E) Detection of neuronal cells mRNA expression *Dlx2* (D) and *Dcx* (E) in FACS-sorted SVZ cells. n = 3–5 samples per cell population, Kruskal-Wallis test followed by permutation test, *: $p<0.05$, **: $p<0.01$. Data are presented in boxplots with medians, minimum and maximum values.

Table 1: Statistical results of qPCR analysis. Related to Figure 2 and Figure S2.
NSC: neural stem cell, TAC: transient amplifying cell

Genes	Kruskal Wallis test	Permutation post test
Gfap	p = 0.02	NSC vs. TAC p = 0.05 NSC vs. Young neuroblast p = 0.03
Nestin	p = 0.19	
Egfr	p = 0.002	NSC vs. TAC p = 0.05 NSC vs. Young neuroblast p = 0.03 TAC vs. Neuroblast p = 0.032 Young neuroblast vs. Neuroblast p = 0.017
Dlx2	p < 0.0001	NSC vs. TAC p = 0.043 NSC vs. Young neuroblast p = 0.014 NSC vs. Neuroblast p = 0.03 TAC vs. Neuroblast p = 0.034 Young neuroblast vs. Neuroblast p = 0.02
Dcx	p = 0.0008	NSC vs. TAC p = 0.019 NSC vs. Young neuroblast p = 0.006 NSC vs. Neuroblast p = 0.015 TAC vs. Neuroblast p = 0.08 Young neuroblast vs. Neuroblast p = 0.07
Scl16a2/Mct8	p = 0.0033	NSC vs. TAC p = 0.024 NSC vs. Young neuroblast p = 0.007 NSC vs. Neuroblast p = 0.019
Sclo1c1/Oatp1c1	p = 0.0047	NSC vs. TAC p = 0.012 NSC vs. Young neuroblast p = 0.004 NSC vs. Neuroblast p = 0.011
Scl16a10/Mct10	p = 0.012	NSC vs. Neuroblast p = 0.032 TAC vs. Neuroblast p = 0.029
Slc7a5/Lat1	p = 0.39	
Slc7a8/Lat2	p = 0.06	
Thra1	p = 0.017	NSC vs. TAC p = 0.015 NSC vs. Young neuroblast p = 0.07 TAC vs. Neuroblast p = 0.036
Thra2	p = 0.021	NSC vs. TAC p = 0.022 NSC vs. Young neuroblast p = 0.014
Klf9	p = 0.0032	NSC vs. TAC p = 0.014 NSC vs. Young neuroblast p = 0.0067 NSC vs. Neuroblast p = 0.022

Supplementary experimental procedures

Olfactory function

The short-term olfactory memory test was performed as previously described (Lazarini et al., 2009). Three WT and five DKO mice were first habituated to a cotton swab and a fresh cage 15 min before the test. Animals were then exposed four times to the same odor for 5 min presentations separated by 2, 30, 60 min intervals. The second presentation is considered as the habituation phase to the odors, and the third and fourth presentations are the memorization phases. This experiment was carried out three times and three different non-social odors were presented to the mice on the cotton swab: almond (vahiné, 1/100), orange blossom (Sainte Lucie, 1/50) and lemon (Sainte Lucie, 1/200). The odor investigation time was measured for each presentation and compared to the first presentation.

Immunohistochemistry

Three to five sections per mice separated by 150 µm along the antero-posterior axis were incubated for 30 min in a blocking solution (10% donkey serum (Sigma), 1% BSA (Sigma), 1X PBS with 0.2% Triton) at room temperature (RT), and then incubated with primary antibodies diluted in the same blocking solution overnight at 4°C. After 3x10 min washes in 1X PBS at RT, sections were incubated with fluorescent secondary antibodies (1/500, Invitrogen) diluted in 1% donkey serum, 1% BSA, 1X PBS with 0.2% Triton. Following 3x10 min washes, sections were incubated with DAPI for 5 min at RT and mounted on glass slides with Prolong Gold antifade reagent (Invitrogen). Antibodies and their dilution factors were as follows: Goat anti-SOX2 (sc-17320), 1:300, Santa Cruz; Rabbit anti-KI67 (AB15580), 1:800, Abcam; Chicken anti-GFAP (AB4674), 1:300, Abcam; Goat anti-DCX (sc-8066), 1:300, Santa Cruz; Guinea Pig anti-DLX2, 1/3000, gift from K. Yoshikawa laboratory; Mouse anti-OLIG2 (MABN50), 1:300, Millipore; Guinea Pig anti-SOX10, 1:300, gift from Mickael Wegner laboratory; Rabbit anti-GFP (sab4301138), 1/300, Sigma; Anti-pan Cadherin antibody [CH-19] (AB6528), 1/500, Abcam; Rabbit anti-MCT8 and anti-OATP1C1, 1:300, gift from T.J. Visser laboratory.

To confirm the localization of MCT8 and OATP1C1 at the cellular membrane, we performed IHC against MCT8 and OATP1C1 together with pan-cadherin on dissociated cells from WT primary neurospheres cultivated as described below. Cells at 24 hours of differentiation were fixed in 100% methanol and blocked with 10% donkey serum and 1% BSA (Sigma Aldrich) in 1X PBS for 30 min at RT. IHC was performed as described above.

Cell migration analysis

To analyse cell migration, primary neurospheres were plated in 8-well glass slides (PEZGS0816, Millicell) coated with Poly-D-Lysine (0.1 mg/ml; Sigma-Aldrich) in growing culture medium without EGF/FGF2 for 3 days. Brightfield images were taken with the EVOS XL Core cell imaging system microscope (x20) and migration distance per neurosphere (µm) was determined using a line drawing tool under FIJI software. The lines are drawn from the outline of the neurospheres to the center of the migrating cells. All cells that migrate from the neurospheres are considered. Migration distances were averaged per neurospheres.

Flow Cytometry and Real-time PCR

The lateral SVZs of five adult WT male mice were dissected and incubated at 37°C in digestion medium containing papain (Worthington), DNase (Worthington), L-cysteine (Sigma-Aldrich) with mechanically dissociation to obtain a single-cell suspension. After the dissociation and resuspension, the cell debris was removed using the Debris Removal Solution (Miltenyi Biotec). Cells were then incubated with a combination of the following antibodies: an Alexa488-conjugated Rat anti-mouse antibody directed against CD133 (Clone 13A4, Thermo Fisher Scientific), a Brilliant Violet 421-conjugated Rat anti-mouse antibody against CD24 (BV421-CD24, BD Biosciences), and an APC-conjugated antibody against EGFR (E13345, Thermo Fisher Scientific) for 30 min at 4°C. Cell sorting was performed on a BD FACS AriaTM III. After 10 min centrifugation at 2,000 rpm, cell pellets of CD133+ EGFR− quiescent NSCs (qNSCs), CD133+ EGFR+ activated NSCs (aNSCs), EGFR+ CD133−CD24− transiently amplifying cells (TACs), EGFR+ CD24+ immature neuroblasts (NPCs), and CD24+ EGFR− migrating neuroblasts were frozen at −20 °C until RNA extraction.

RNA extraction and reverse-transcription were done using the RNAqueous-Micro kit with DNase treatment (ThermoFisher) and the Reverse Transcription Master Mix from Fluidigm, following the manufacturer's instructions. Pre-amplifications were performed for genes of interest using the Taqman Preamp Master Mix kit (ThermoFisher), with primers from Taqman. Gene expression assays: *Slc16a2/Mct8* (mm00486204_m1); *Slco1c1/Oatp1c1* (mm00451845_m1); *Slc16a10/Mct10* (mm00661045_m1); *Slc7a5/Lat1* (mm00441516_m1); *Slc7a8/Lat2* (mm01196249-m1); *Thra1* (Nm178060.3); *Thra2* (BC046795.1); *Klf9* (Mm00495172_m1); *Gfap* (mm01253033_m1); *Nestin* (Mm01223404_g1); *Egfr* (mm01187858_m1); *Dlx2* (mm00438427_m1); *Dcx* (mm00438400_m1); *Gapdh* (mm99999915_g1); *Actb* (mm00607939_s1). RTqPCR reactions were performed in triplicate for each sample using Reverse Transcription Master Mix (Fluidigm) on a QuantStudioTM6 Flex Real-Time PCR System (Applied Biosystems), following manufacturer recommendations. The Ct's were averaged and

normalised (ΔCt) against the geometric mean of two reference genes (Gapdh and Actin beta). Variations of expression were quantified by the ΔΔCt method (Livak KJ, Schmittgen TD (2001)). Analysis of relative gene expression data was done using real-time quantitative PCR and the 2(-ΔΔCt) Method.